Comparison of size and morphological measurements of coarse mode dust particles from Africa

Jeffrey S. Reid,[1,2] Halflidi H. Jonsson,[3] Hal B. Maring,[4] Alexander Smirnov,[5] Dennis L. Savoie,[4] Steven S. Cliff,[6] Elizabeth A. Reid,[7] John M. Livingston,[8] Mike M. Meier,[9] Oleg Dubovik,[5] and Si-Chee Tsay[10]

Received 26 April 2002; revised 30 July 2002; accepted 11 August 2002; published 12 July 2003.

[1] A multitude of sensitivity studies in the literature point to the importance of proper chemical and morphological characterization of particles when the radiative impacts of airborne dusts are modeled. However, the community data set is based on heterogeneous measurement methods relying on varying aerodynamic, chemical, morphological, and optical means. During the Puerto Rico Dust Experiment, size distributions of dust particles from Africa were measured using a variety of aerodynamic, optical, and geometric means. Consistent with the literature, comparisons of these size distributions showed quite dissimilar results. ''Measured'' volume median diameters varied from 2.5 to 9 μm for various geometric, aerodynamic, optical, and optical inversion methods. Aerodynamic systems showed mixed performance. Column integrated size distributions inverted from AERONET Sun/sky radiance data produced somewhat reasonable results in the coarse mode when given proper constraints and taken in the proper context. The largest systematic errors were found in optical particle counters due to insensitivities to particle size in the 4–10 μm region with further complications due to dust particle morphology and index of refraction issues. As these methods can produce quite dissimilar size distributions, considerable errors in calculated radiative properties can occur if incorrectly modeled into dust parameters. None of the methods compared in this study can adequately reproduce the measured mass extinction or mass scattering efficiency of the dust using spherical geometry methods. Given all of the uncertainties in the sizing methods, we promote the use of fundamental and quantifiable descriptors of particles such as mass as a function of aerodynamic diameter. *INDEX TERMS:* 0305 Atmospheric Composition and Structure: Aerosols and particles (0345, 4801); 0330 Atmospheric Composition and Structure: Geochemical cycles; 0360 Atmospheric Composition and Structure: Transmission and scattering of radiation; 0368 Atmospheric Composition and Structure: Troposphere—constituent transport and chemistry; *KEYWORDS:* dust, measurement, impactor, optical particle counter, inversion, size distribution

Citation: Reid, J. S., et al., Comparison of size and morphological measurements of coarse mode dust particles from Africa, *J. Geophys. Res.*, *108*(D19), 8593, doi:10.1029/2002JD002485, 2003.

1. Introduction

[2] There are numerous studies in the literature conveying sensitivity studies on the impact of uncertainties in dust particle size, chemistry and morphology on dust optical and radiative properties. These studies include the impact of particle nonsphericity [e.g., *Mishchenko and Travis*, 1994; *Mishchenko et al.*, 1997; *Pilinis and Li*, 1998; *Kalashnikova and Sokolik*, 2002], particle size and refractive index variability [e.g., *Patterson*, 1981; *Tegen and Lacis*, 1996; *Claquin et al.*, 1998; *Schulz et al.*, 1998; *Myhre and Stordal*, 2001], and vertical distribution and transport mechanisms [e.g., *Westphal et al.*, 1987; *Liao and Seinfeld*, 1998; *Quijano et al.*, 2000a, 2000b; *Ginoux et al.*, 2001; *Myhre and Stordal*, 2001]. Indeed, such scrutiny is necessary, as airborne dust is a heterogeneous mix of particles with radically different properties. Particle chemistries vary from region to region and Asian dusts can be dissimilar from those from the Sahara region [*Ganor et al.*, 1991; *Sokolik*

[1]Space and Naval Warfare Systems Center-San Diego, San Diego, California, USA.
[2]Now at Naval Research Laboratory, Monterey, California, USA.
[3]Naval Postgraduate School, Monterey, California, USA.
[4]Rosenstiel School of Marine and Atmospheric Science, University of Miami, Miami, Florida, USA.
[5]GEST Center, University of Maryland, Baltimore County, Baltimore, Maryland, USA.
[6]DELTA Group, Applied Science, University of California, Davis, California, USA.
[7]Naval Research Laboratory, Monterey, California, USA.
[8]SRI International, Palo Alto, California, USA.
[9]Material Science and Chemical Engineering, University of California, Davis, California, USA.
[10]NASA Goddard Space Flight Center, Greenbelt, Maryland, USA.

0148-0227/03/2002JD002485$09.00

and Toon, 1999; *Gao and Anderson*, 2001]. Even within a given source region, say the Sahara, individual particles such as clay minerals and other alumino-silicates can have widely varying shapes, chemistries, and hence optical properties [*Coude-Gaussen et al.*, 1987; *Anderson et al.*, 1996; *Falkovich et al.*, 2001; *Koren et al.*, 2001].

[3] Unlike other aerosol types where spherical particle approximations are more or less valid (such as hydrated sea-salt, biomass burning, and fine mode anthropogenics), dust particles pose tremendous challenges in radiative and global climate models. Detailed microphysics and chemistry are regularly sacrificed in these models in favor of computational expedience. Even so, *Mishchenko et al.* [1997] suggested that compared to elongated spheroids, the use of the spherical model can adequately reproduce particle extinction. Difficulty begins to arise in computing the dust's scattering phase function [*Dubovik et al.*, 2002b; *Kalashnikova and Sokolik*, 2002], and by implication single-scattering albedo. Dust mass scattering efficiency also becomes more variable due to calculated mass/volume/density uncertainty. As particle deposition velocities become significant for coarse mode particles, the mass extinction efficiency may become more uncertain with distance [e.g., see *Westphal et al.*, 1987]. Further, there is very little experimental data (particularly in the IR portion of the spectrum) for theory verification. Based on all of the uncertainties listed above it is still not clear whether airborne dust has a heating or cooling effect on the atmosphere globally [e.g., *Intergovernmental Panel on Climate Change* (*IPCC*), 2001; *Myhre and Stordal*, 2001].

[4] Compounding all of the physical uncertainty in dust particles are the uncertainties in the measurement methods. Ultimately most particle size methods, whether aerodynamic, optical, or morphologic, trace their initial calibration and validation back to some form of a uniform spherical model. For example, aerodynamic methods that utilize the ''aerodynamic'' diameter trace back to the aerodynamic properties of an equivalent unit density sphere. Optical methods trace back to the angular scattering properties of polystyrene or glass beads of known index of refraction. Morphologically, the diameter of equivalent volume or cross sectional area is commonly used. Aside from issues related to particle asymmetry, density, and index of refraction, sampling bias for coarse mode particles can also be a significant issue. High wind speeds commonly found during dusty conditions can cause particle losses or enhancement in sampling inlets [*Brockman*, 1993]. Aircraft observations of the coarse mode also suffer from poorly characterized inlets and airflow uncertainties [*Brock et al.*, 1993]. Hence, when modeling the radiative effects of airborne dusts one must be extremely careful when interpreting and applying field measurements. Understanding the impact of airborne dust on the atmosphere's radiative balance will come from a combination of remote sensing and modeling that depends on some form of particle size parameterization that can be efficiently utilized. Given the uncertainty in such parameterizations, it is unclear what parameterization should be used and what the true uncertainty is.

[5] The Puerto Rico Dust Experiment (PRIDE) was a joint Office of Naval Research (ONR) and National Aeronautical and Space Administration (NASA) funded field study conducted on the eastern side of the island of Puerto Rico [*J. S. Reid et al.*, 2003]. Based at Naval Station Roosevelt Roads, participating investigators monitored Saharan dust transport across the Northern Tropical Atlantic Ocean between 28 June and 24 July 2000, utilizing a variety of airborne, satellite, and surface instrumentation. As discussed in other papers on the PRIDE campaign, the island of Puerto Rico was in the center of the dust transport plume from Africa during the study. Daily averaged dust optical depths at 500 nm averaged 0.24, with a maximum of 0.52. Dust concentrations at the surface were at times greater than 70 $\mu g\ m^{-3}$.

[6] The purpose of PRIDE was twofold. First, participating scientists wished to better understand the nature of dust transport in order to evaluate/validate dust transport models such as the Naval Research Laboratory Aerosol Analysis and Prediction System (NAAPS-http://www.nrlmry.navy.mil/aerosol) and the NCAR Model for Atmospheric Transport and Chemistry (MATCH) [*Colarco et al.*, 2003]. Second, PRIDE was to investigate the extent to which the microphysical, chemical and optical properties of dust particles need to be known before remote sensing systems can accurately determine dust optical depth and radiative flux. That is to ask whether dust microphysical properties need to be known before remote retrievals become meaningful or if there is some cancellation of errors or insensitive method that can be exploited. In this study we are most concerned with the latter goal. In particular, we investigate the extent to which particle size distributions can even be characterized and the uncertainties size parameterizations have in model and satellite investigations. This is done for single particle analysis, cascade impactors, aerodynamic particle sizers, optical particle counters and Sun/sky inversions.

2. Background on Measured Size Distributions and Radiative Effects of Dust

2.1. Sizing Issues and Definitions

[7] All particle-sizing methods are based on the quantifiable measurement of some physical aspect of the particle. Loosely, these can be categorized by their geometric (physical size), aerodynamic (related to their mass and aerodynamic drag), or optical (light scattering and extinction) properties. Typically measurements are related to some equivalent ''spherical'' or ''ellipsoid'' size distributions. Examples of reported dust size distributions from these various methods are presented in Table 1. In the sections 2.1.1–2.1.4 we give a brief overview of the most commonly used methods.

2.1.1. Geometric Sizing

[8] Geometric size distributions are commonly made using electron and some light microscopy techniques. Examples of detailed analysis of dust are given by *D'Almeida and Schutz* [1983], *Coude-Gaussen et al.* [1987], *Reid et al.* [1994a], *Anderson et al.* [1996], *Gao and Anderson* [2001], and *Koren et al.* [2001]. Transmission, backscatter, or secondary electron images are generated, from which individual particles are measured. Measuring can be done manually or by computer. As images are two dimensional, an equivalent cross sectional area sphere or spheroid is typically used. Particle's cross sectional surface area, perimeter, or the major-minor axes are reported. For expediency the 2 dimensional image is often all that is used

Table 1. Reported Volume/Mass Distributions for Transportable Dust Particles[a]

Study	Region	MMD, μm	VMD, μm	Geometric Standard Deviation σ_g
		Aerodynamic Methods		
Arimoto et al. [1997]	remote oceans	3 ± 1		2–4
D'Almeida [1987]	Sahara	3 ± 1		2.1
Gomes et al. [1990]	Algeria	3 ± 0.5		1.8
Gomes and Gillette [1993]	Tadzhikistan	3–6		–
Gullu et al. [1996]	Turkey (from Libya)	7 ± 1		–
Maenhaut et al. [1999]	Negev desert	5 ± 1		–
Maring et al. [2000]	Canary Islands	5 ± 1		
Patterson and Gillette [1977]	Texas	6 ± 1		2.2
Reid et al. [1994b]	Owens (Dry) Lakebed	4 ± 1		2.3
Sviridenkov et al. [1993]	Tadzhikistan	5 ± 1		1.9 ± 0.3
Talbot et al. [1986]	Barbados	3.2 ± 0.8		2.5
PRIDE study	Puerto Rico (Saharan)	3.5 ± 1		2.0
Mean		4.5 ± 1.3		2.1 ± 0.2
		Optical Counter Methods		
Ackerman and Cox [1982]	Arabian Sea		12 ± 2	~2
Cahill et al. [1994]	Owens (Dry) Lake		>5	-
Carlson and Caverly [1977]	Capo Verde		13 ± 2	2.1
Collins et al. [2000]	Tenerefe		>8	-
Fouquart et al. [1987]	Niger		>6	
Levin et al. [1980]	Israel		>5	-
Porter and Clarke [1997]	Hawaii (Asian)		6.5 ± 1[b]	2.2
Sviridenkov et al. [1993]	Tadzhikistan		9 ± 1	2.0
PRIDE study	Puerto Rico (Saharan)		9 ± 1	1.5
Mean			>9	~2.0
		Optical Inversion Methods		
Dubovik et al. [2002a]	various		3.8–5.2	–
Kaufman et al. [1994]	Israel		3.0–5.0	–
Smirnov et al. [1998]	Tenerefe		4.5 ± 1	~2.0
Smirnov et al. [2002]	Bahrain		5.5 ± 1	2.1 ± 0.2
Tanre et al. [2001]	Western Africa and Israel		5–7	–
Mean			5 ± 1.5	~2.0

[a]Values from aerodynamic methods were measured by cascade impactors, except for *Maring et. al.* [2000], which used an aerodynamic particle sizer. Given is the mass median diameter (MMD) (aerodynamic) and geometric standard deviation (σ_g). Optical counter methods include optical particle counters such as PMS and the Royco spectrometer probes. For optical probes the volume median diameter (VMD) (optical equivalent) and, σ_g are given. Optical inversion methods list studies that utilized inversions based on AERONET Sun/sky radiance measurement. Optical equivalent volume median diameter and geometric standard deviation are given.
[b]Estimated from given surface median diameter and geometric standards deviation using Hatch-Choat equations.

along with a qualitative description, although shadowing methods can give some 3-D information for transmission microscopy.

[9] Microscopy methods suffer from several setbacks. Most importantly one must ensure proper counting statistics. The most particle volume in the coarse mode is usually associated with the largest 1% of particles. Hence many thousands of particles at multiple magnification levels must be measured on each sample if proper size statistics are to be made. A multitude of statistics can be generated including cross sectional area, equivalent sphere size, orthogonal major and minor axes, maximum and minimum dimensions, the ratio of surface area to circumference, and many more. Ratios of these variables can be used to categorize some particle morphologies (e.g., the ratio of cross sectional area to perimeter [*Koren et al.*, 2001]). However, each particle is usually interpreted as a spheroid and the real character is lost. Aside from the computation and analysis of these statistics being labor intensive, there is some subjectivity in interpreting and presenting the data. This makes regular electron micrograph studies expensive and results difficult to implement into models.

[10] A second issue is in the collection of the particles. Since collection is on a filter or electrostatic/thermal precipitator, particles typically are oriented such that their minor axis is normal to the substrate. More simply, the largest flat side is face down. Thus, for species such as clay elements that are typically flat platelets, sizes are biased high. Similarly, semiliquid particles such as hydrated sulfates and some organics will flatten on the surface leaving a halo. In these cases particle sizing can be biased high or low depending on if the outer halo or inner particle is used.

2.1.2. Aerodynamic Sizing

[11] Aerodynamic sizing methods segregate particles based on their mass-to-drag characteristics. By definition, the aerodynamic equivalent diameter (or simply aerodynamic diameter), d_{ae}, is the diameter of a unit density sphere that has the same settling velocity of the particle in question. For spheres the settling velocity is given by [*Hinds*, 1982]:

$$V_{grav} = \frac{g\rho_p d_p^2 C_c}{18\eta} \quad (1)$$

where g is the gravitational constant (980 cm s^{-1}), ρ_p is the particle density, d_p is the particle diameter, C_c is the Cunningham slip correction (equal to 1 for particles greater than ~1 μm), and η is the viscosity (182 μP at STP). Hence for spheres the particle diameter is equal to the aerodynamic

diameter divided by the square root of the density. Dust component densities vary, but values include amorphous silicon oxide (2.1–2.3 g cm^{-3}), illite/muscovite (~2.7–3.1 g cm^{-3}), montmorillonite (2.2–2.7 g cm^{-3}), and quartz (2.65 g cm^{-3}).

[12] Because most coarse mode particles are not spheres, a dynamic shape factor, χ, is added to account for changes in the particle's drag coefficient:

$$V_{grav} = \frac{g\rho_p d_p^2 C_c}{18\eta\chi} \quad (2)$$

When χ is included in calculations, the conversion between d_p and d_{ae} for coarse mode particles becomes

$$d_p = d_{ae}\sqrt{\frac{\chi}{\rho_p}} \quad (3)$$

[13] Values of χ vary in a wide range for differing dust particle shapes. For example, *Davies* [1979] found $\chi = 1.12$, 1.27, and 1.32 for double, triple and quadruple chained spheres. For more dust-like species, they found $\chi = 1.36$–1.82 for quartz, 2.04 for talc and 1.57 for "sand" like species. Given these values and the densities listed above, conversions between d_p and d_{ae} are probably in the range of 1.2 to 1.5. However, it is immediately clear that equation (3) is ambiguous. How is d_p defined for an irregular particle? Generally it is taken as a sphere of equivalent volume, although this approximation obviously becomes less valid for more irregular particles.

[14] The two most common aerodynamic methods used to measure dust particle size are cascade impactors and various forms of aerodynamic particle sizers (see *Marple et al.* [1993] and *Baron et al.* [1993] for complete discussions). Cascade impactors collect particles passing through a jet onto a collection substrate. Those particles which are "aerodynamically large" impact on the surface and stick. Smaller particles can flow around the substrate and into the next stronger jet and can be collected on subsequent substrates. These substrates are then removed for gravimetric, chromatographic or elemental analysis.

[15] Aerodynamic particle sizers (APS) also gauge size based on atmospheric drag. Like impactors, particles are accelerated through a jet. Particle velocities are then measured at some distance away from the jet outlet. Larger particles with higher inertia or high mass to drag ratios accelerate through the jet more slowly than smaller particles. Particle velocities are then compared to some calibration curve. Unlike the impactors, which measure the total mass concentrations of the aerosol particles or species, APS instruments are single particle counters measuring number concentrations. As will be shown in later sections, this is an important distinction.

[16] Aerodynamic methods have their own set of analysis issues. In particular the relationship in equation (3) is not straightforward. As dust is a heterogeneous mix, the ratio of ρ_p to χ is unique for each particle and natural separation can occur. Also, impactors can suffer from bounce off, where particles that should have been collected on a substrate bounce off on impact and are collected on other substrates down the stream. Particle orientation issues can also widen measured size distributions. Because aerodynamic particle sizers accelerate particles to high velocities in jets, particles of unusual shapes such as dust can cause biases.

2.1.3. Optical Particle Counters

[17] Optical particle counters (OPC) size particles by measuring the amount of light scattered off of individual particles transiting a beam of light into some detector (see *Rader and O'Hern* [1993] for a discussion). Sizing occurs by comparing the pulse height from the detector to a calibration curve derived by calibration with spheres of known size and refractive index. An optical equivalent diameter, d_{oe}, is assigned. In order to derive correct size, corrections must be made for particle index of refraction and shape.

[18] Each OPC on the market has its own geometry for measuring particle light scattering. Most use coherent light sources (i.e., lasers) at single wavelengths. Scattering viewing volumes range from the far forward (e.g., the Forward Scattering Spectrometer Probe (FSSP), 4–12°), midrange (e.g., active scattering aerosol spectroscopy probe (ASASP), 35–120°), and even backscatter (cloud aerosol precipitation spectrometer, CAPS). Each instrument has its own correction factor for particle index of refraction. Like the other geometric and aerodynamic methods sizing becomes ambiguous for particles with mixed chemistries and irregular shapes.

2.1.4. Optical Inversion Methods

[19] Inversions from spectral remote sensing data (surface or space-borne) are used to estimate particle properties based on spectral extinction and angular scattering information [e.g., *Nakajima et al.*, 1996; *Dubovik et al.*, 2000]. Typically, spectral extinction or sky radiance data are compared to a variety of particle size distributions and chemistries and the "best fit" distribution is used. Unlike the in situ methods the retrieved size distributions are not anchored to any microphyscial parameter such as number or mass concentration, but rather are constrained to optical depth and sky radiance. Hence "column closure" is forced to occur.

[20] Inversion methods derive information from integrated columns and hence give integrated values. Thus, if the column is a mix of various particle types and sizes a distribution representing the sum through column is presented. It must also be understood that these inversions are a best fit to the sky radiance field and solution degeneracy can exist. A significant constraint in these methods is that they can only be used in relatively clear sky conditions. While cloud screening algorithms remove most cloud contaminated samples, cirrus contamination can take place.

2.2. Dust Properties

[21] *Patterson and Gillette* [1977], *D'Almeida and Schutz* [1983], and *Gomes and Gillette* [1993] noted commonalties in dust particle size distributions measured over differing arid portions of the globe. Utilizing data from cascade impactors (that is, measuring particle mass as a function of aerodynamic diameter), these investigators found that airborne dust typically has two mass modes: a prominent giant mode with a mass median diameter (MMD) >40 μm, and a mode created by the saltation processes with a MMD between 3–6 μm. It has also been suggested that sometimes

a third submicron mode can also be present [*Gomes et al.*, 1990; *Reid et al.*,1994b].

[22] Because particles in the giant mode fall out relatively quickly, most attention has been paid to the more transportable saltation formed mode in the 3–6 μm range. Table 1 lists commonly cited coarse mode particle mass/volume distributions from the literature. Values are separated by measurement method: aerodynamic methods for impactors and aerodynamic particle sizers, optical counter methods for optical particle counters, and optical inversion methods for Sun/sky inversions. Values are for aerodynamic and optical equivalent diameters. Generally, the aerodynamic and inversion methods group into the same size range. Regardless of location or investigator the MMD is consistently in the 3 to 6 μm region, and the geometric standard deviation is on the order of 2. Dusts from source regions in, say, Algeria are not dissimilar to those of a dry lakebed. Across the literature, the average aerodynamic MMD for dust collected by aerodynamic means is ~4.3 μm (aerodynamic). Given the discussion in section 2.1.2 this would imply a mean geometric MMD of ~3 μm. However, size distributions determined by use of optical particle counters suggest a more varied nature and a much larger size. Consistently, investigators utilizing optical particle counters in similar regions of the world derive volume median diameters on the order of 8–13 μm, 2–3 times greater than aerodynamic and inversion methods. Consider the reported values of *Sviridenkov et al.* [1993] for dust in Tadzhikistan, where using aerodynamic and optical means simultaneously the same factor of 3 difference was observed. Similarly, the aerodynamic MMD from Owens (dry) lake presented by *Reid et al.* [1994b] is at least half the value of the simultaneous optical measurement by *Cahill et al.* [1994]. Clearly, there is a systematic difference between the two methods in the literature.

2.3. Size Variance Impacts

[23] Even a relatively small amount of variability in particle sizes can cause drastically different results when applied in radiative transfer algorithms. The nature of dust variability on direct forcing is well illustrated in Figure 1, where the volume extinction efficiency α_{ve}, (in m^2 cm^{-3}) and single scattering albedo (ω_o) is plotted against wavelength. This is done for various lognormal distribution volume median diameters and a constant geometric standard deviation of 2 (typical for dust). The index of refraction as a function of wavelength of *Shettle and Fenn* [1979] is used. These values have been disputed and result in single scattering albedo values that are likely to low. It is often assumed that spherical scatterers cause no more than a 10% error in this calculation [*Pilinis and Li*, 1998], although we present contrary evidence later. However, for this simple illustration on trends, these assumptions suffice.

[24] Examination of Figure 1 demonstrates the findings of a multitude of dust sensitivity studies [*Tegen and Lacis*, 1996; *Claquin et al.*, 1998; *Liao and Seinfeld*, 1998; *Myhre and Stordal*, 2001]. For shortwave radiative forcing (midvisible), variations in particle size can have a dramatic impact in α_{ve}. In the shortwave Q_{ext} is roughly two for all coarse mode particles. Hence α_{ve} varies as the ratio of surface area to volume, (or d_p^{-1}). So α_{ve} can increase by a third for a VMD change of say 6 to 4 μm, and can increase by a further factor of two for a change of 4 to 2 μm (It is noteworthy here that aerodynamic methods place the saltation created mode in the center of this range!). Similarly, ω_o varies considerably with size as less internal refraction occurs for larger particles. However, in the midinfrared ($\lambda > 3.4$ μm), there is considerably less impact on α_{ve} and ω_o from size variability for particle sizes larger than ~3 μm (<25%). At these longer wavelengths, Q_{ext} grows and counteracts the d_p^{-1} dependence and the wavelengths become on the order of particle size so particle refraction can occur. Conversely, any shift in complex index of refraction in the infrared will disrupt the derived value of ω_o and have a dramatic impact on longwave forcing.

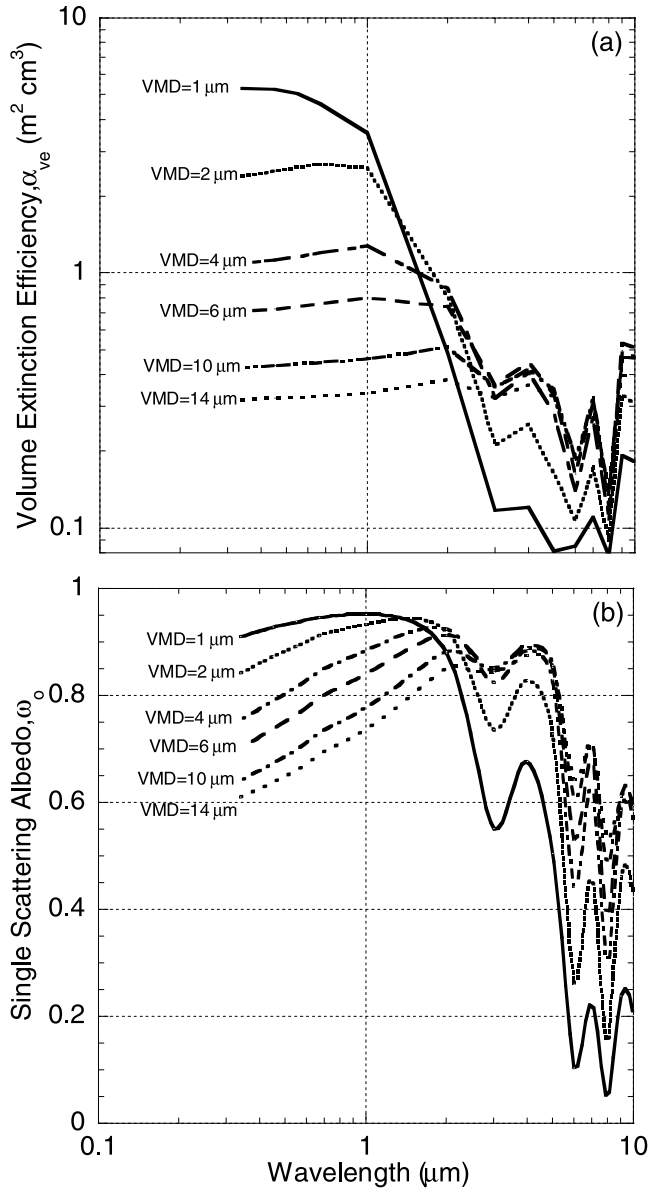

Figure 1. Calculated (a) volume extinction efficiencies and (b) single-scattering albedo as a function of wavelength computed for spherical lognormal size distributions with various volume median diameters and a constant geometric standard deviation of 2. The index of refraction of *Shettle and Fenn* [1979] is used.

[25] Extending this short analysis indicates one of the principal difficulties in modeling the impact of dust is understanding the true uncertainties in the size parameters used. Given the difference in the mean value of dust particles sizes listed in Table 1, the variability in α_{ve} is a factor of 4, and in absorption is a factor of 2. Even within the standard deviation of the mean value for only the aerodynamic methods (3 ± 1 μm, after converting to a geometric distribution), there is still a ~35% uncertainty.

3. PRIDE Field Study Design and Instrumentation

[26] As part of the PRIDE field campaign a surface station with an extensive radiation and aerosol microphysics package was installed on Cabras Island (latitude ~18.21°N, longitude ~65.60°W). See *J. S. Reid et al.* [2003] for a description. The University of Miami maintained a laboratory trailer with instrumentation that included nephelometers, absorption photometers, an aerodynamic particle size spectrometer, and filter/cascade impactor samplers [*J. S. Reid et al.*, 2003; D. L. Savoie et al., Spectrally-resolved light absorption by Saharan aerosols over the tropical North Atlantic, submitted to *Geophysical Research Letters*, 2003 (hereinafter referred to as Savoie et al., submitted manuscript, 2003)]. Continuous mass measurements were made with a tapered element oscillating microbalance (TEOM) (Savoie et al., submitted manuscript, 2003). NASA maintained a separate station of radiometric instrumentation including a micropulse LIDAR, an Aerosol Robotic Network (AERONET) Sun photometer, and broadband, direct/diffuse, and shadow band radiometers.

[27] Aircraft operations were conducted by a twin-engine, 8-seat piper Navajo owned and operated by Gibbs Flite Center and contracted by Space and Naval Warfare Systems Center San Diego. A complete description of the Navajo payload and flight plan is given by *J. S. Reid et al.* [2003]. Additional airborne operations were conducted by the University of Miami Cessna (a full description of the Cessna package and performance is discussed by *Maring et al.* [2003b] and is not discussed in this paper). In the following sections we review the instrumentation used in this intercomparison.

3.1. Cascade Impactors

[28] Two cascade impactors were deployed during PRIDE at the Cabras Island site and sampled air at ambient relative humidity. The first was a University of Miami Micro-Orifice, Uniform-Deposit Impactor (MOUDI) collecting 24 hour samples in 8 stages with 50% cut points at 22, 12, 7.6, 3.8, 2.2, 1.24, 0.71, and 0.41 μm (Savoie et al., submitted manuscript, 2003). Sampler flow was at 30 Lpm. Samples were subjected to ion chromatography analysis to obtain major ions (Na^+, Cl^-, K^+, Ca^{2+}, NO_3^-, $SO_4^=$). One integrated 68 hour sample on ungreased Whatman 41 substrates from within the 21 July the 24 July period was subsequently analyzed by neutron activation analysis (NAA) to determine Al, Br, Cl, Mn, Na, V, I, and K. Comparisons with bulk filter samples suggest that the impactor was loosing 30–40% of sea-salt mass at the largest sizes either through inlet issues or a bad o-ring seal. This is discussed in the results section.

[29] Also at the Cabras Island site was a Davis Rotating Drum (DRUM) impactor owned by investigators from the University of California, Davis. The DRUM sampler collects particles in eight stages with 50% cut points at: 5 μm, 2.5 μm, 1.1 μm, 0.74 μm, 0.56 μm, 0.34 μm, 0.24 μm, 0.07 μm in diameter, for the eight stages, respectively. This sampler was slightly modified from the original version of *Cahill et al.* [1985], by using a slit inlet (instead of a jet) and flow rate was increased from 5 to 10 liters per minute. Samples were collected on Apeazon grease coated strips on rotating drums moving at ~1 mm each 4 hours (3–24 July) giving 4 hour resolution. After collection, sample strips were subjected to X-Ray Fluorescence (XRF) analysis at the Advanced Light Source of Lawrence Berkeley National Laboratory to measure elements Na through Cu. However, the Na was at the end of the usable range and the data had relatively high uncertainties. For example, while sodium and chlorine correlated very well (r = 0.9) the chlorine to sodium ratio was 2, higher than the nominal value of 1.5 for aged sea-salt particles.

3.2. Aerodynamic Particle Sizer

[30] Coarse mode particle sizing at the University of Miami trailer was performed using a TSI aerodynamic particle sizer (APS) 3310 from 2 to 24 July [*Baron*, 1986; *Maring et al.*, 2003b]. This instrument bases particle size on the particles aerodynamic behavior by measuring the rate of acceleration of particles moving through a jet. This rate is compared to calibrations using glass beads. During PRIDE the APS measured particle diameter between 0.8 to 30 μm in integrated 20-minute samples. The APS was plumbed to the main aerosol inlet of the trailer and the airflow was dried to a relative humidity below 50%. The critical and defining parameter for correct calibration in the APS is airflow rate through the system. The APS's internal flowmeters were directly calibrated with a bubble flowmeter weekly. Flow rates in the APS were checked and, if necessary adjusted at least 3 times per day. Glass bead calibrations occurred 3 times during the study.

3.3. AERONET Sun Photometer

[31] Two Aerosol Robotic Network (AERONET) Sun photometers were deployed on Puerto Rico for the PRIDE campaign. The principal one was at the Cabras Island site for the duration of the study. The second, installed on 1 July 2001, is still operating at La Paguera, on the south west corner of Puerto Rico (18.0°N, 67.0°W). The AERONET Sun photometers measured spectral aerosol optical depth (τ_a) at seven wavelengths (340, 380, 440, 500, 675, 870 and 1020 nm) for aerosol particle extinction plus water vapor from a 940 nm channel [*Holben et al.*, 1998, 2001]. Optical depth data were taken every 15 minutes, and sky radiance measurements every hour. Both instruments have undergone pre and poststudy calibrations. Cloud screening was performed using the *Smirnov et al.* [2000] scheme with requirements that include stable aerosol optical thickness (AOT) values within a 1 minute period (allowed variability is 0.02 for AOT less than 0.667 or 0.03 τ_a for greater AOT), and limited variations of the second derivative of the logarithm of AOT as a function of time. *Smirnov et al.* [2000] notes that thin uniform cirrus may not be screened using this algorithm.

[32] In addition to spectral measurements of τ_a, AERONET Sun/sky radiometers also measure the angular distribution of sky radiances in 4 wavelengths (440, 675, 970, and 1020 nm). Utilizing both the spectral τ_a data in these wavelengths and the sky radiances in the almucantar scans, the *Dubovik and King* [2000] algorithm was employed to compute retrievals of aerosol particle size distribution (in the range of 0.1 μm < d_p < 30 μm) and refractive indices. These aerosol parameters are utilized in Mie computations to derive the aerosol particle ω_o. A full description of the inversion quality control techniques is presented by *Dubovik et al.* [2002a]. The minimum solar zenith angle suggested is 20° and the almucantar scan checks for symmetry at 21 angular points to remove cases with thin cirrus. *Dubovik et al.* [2000] found that *Dubovik and King* [2000] inversion can be susceptible to particle asymmetry effects. If sky radiance data from >60° scattering angles are used (that is solar zenith angles (ζ) greater than 30°), an anomalous fine mode peak is derived to compensate for the additional scattering asymmetric particles produce at scattering angles >120°. *Dubovik et al.* [2000] found that this anomalous peak did not affect the coarse mode retrieval. Also, *Dubovik et al.* [2000] suggests ω_o values are reliable (±0.03) when $\tau_{a440} > 0.5$. Recently, *Dubovik et al.* [2002b] developed code that accounts for particle nonsphericity. As we will show, these new calculations did not modify the size or shape of the coarse mode calculations discussed here. The ''goodness of fit'' of the inversions is tested by comparing Mie calculations of the retrieved size distribution to the measured radiance fields. Reproductions with 5% are considered good. In this study we only utilize retrievals that meet this requirement.

[33] For comparison, the *Nakajima et al.* [1996] inversion was also run on those *Dubovik and King* [2000] inversions that converged. Unlike the Dubovik and King inversion, in the Nakajima inversion the index of refraction is fixed and data from >140° scattering angles (>60° solar zenith angles) are not utilized. As the Nakajima inversion does not utilize optical depth, in some cases AOT is not necessarily reproduced in the inversion, although this was not the case for this study.

3.4. Navajo Operations with PMS Probes

[34] A complete description of the Navajo and its flight plans is given by *J. S. Reid et al.* [2003]. However, a short overview is presented here. For the PRIDE study, the Navajo carried basic meteorological instrumentation (Rosemount temperature ±0.3°C, EGG dew point ±0.5°C, Vaisala relative humidity ±5% and temperature ±0.3°C, and static pressure ±0.2 mb), plus the NASA Ames hyperspectral radiometers to measure up-welling and down-welling flux, and a 6 channel airborne Sun photometer to measure aerosol optical thickness [*Matsumoto et al.*, 1987]. A polycarbonate filter sample was taken through a small isokinetic inlet for electron microscopy. Two aerosol particle probes, the Particle Measuring Systems (PMS) FSSP-100 (Forward Scattering Spectrometer Probe) and PCASP-100X (Passive Cavity Aerosol Spectrometer Probe), were mounted on the Navajo wingtips. During PRIDE, the Navajo flew 21 flights (61 hours of data collection over eighty flight hours) near the islands of Puerto Rico, St. Thomas, and St. Croix. Each flight began with a continuous vertical profile (~30 m to 5000 m) over the aerosol/radiation site to characterize the local environment. It is from this portion of the flights the data presented in this study is derived.

[35] Both the FSSP-100 and PCASP-100X had undergone the Droplet Measurement Technologies, Inc. electronics upgrades. Nominally, the FSSP and PCASP measured particle size in 20 channels from 0.75 to 18 μm and 0.1 to 3 μm in diameter, respectively. The PCASP samples particles from an inlet into a closed cavity at a rate of 1 cm^3 s^{-1}. The PCASP sizes particles based on particle light scattering (35–135°) in a 633 nm HeNe laser beam. The inlet deicing heater for the PCASP was on during the study such that the instrument would give a dry particle size distribution (RH = 35–40%). The FSSP-100 gives an ambient size distribution based on 633 nm light scattering in the 4–12° range. The FSSP-100 is an open celled instrument and ram air passes through an open sampling volume. At a nominal 55 m s^{-1} airspeed the sampling volume is ~17 cm^3 s^{-1}.

[36] Calibrations were conducted before and after deployment and are based on glass beads and polystyrene spheres for the FSSP and PCASP, respectively. Two additional calibrations were performed in the field in the first and last week of the study. Plots of particle calibration points on theoretical response curves to calibration particles are presented in Figure 2. The field calibrations for the FSSP-100 compared extremely well, suggesting that the calibration remained stable throughout the study. The PCASP was also stable, although some anomalous insensitivity was found in the 0.4–0.8 μm range compared to theory (solid line). We have found that this anomaly is consistent between instruments, and is likely due to a gain shift in the instrument in the 0.3–0.5 μm range. This was corrected for in the calibration.

3.5. Microscopy

[37] Airborne polycarbonate filters were collected on the Navajo through a small 1 cm isokinetic inlet sampling at 5 Lpm. These filters were subjected to scanning electron microscopy (SEM) and energy-dispersive analysis with X rays (EDX) analysis at the University of California, Davis Materials Science Department microscopy lab. An EDAX Phoenix Energy Dispersive Spectrometer (EDS) system was used to collect the X-ray spectra. The samples were prepared by removing a pie shaped wedge representing about one eighth of the total filter area from each aircraft filter. Strips were mounted on aluminum stubs with double-sided carbon tape, then carbon coated with 30 nm of carbon. The samples were first previewed in an ISI DS-130 SEM with an Oxford ISIS 200 EDS system with a Be window. Particle sizing was performed both by computer and by hand using polygonal mapping. Particle area, circumference, and orthogonal major and minor axes were recorded. Major and minor axes are derived from a best fit ellipse. EDX was performed with an Oxford instruments EDS detector with a Be window. The EDX analysis gave semiquantitative estimates of the relative concentration for the elements Na through Cu. Both secondary electron and backscatter images were used in the analysis.

4. Measured Size Distribution Comparisons

4.1. Geometric Properties of Dust Particles

[38] Before a detailed comparison of dust measuring techniques is performed, it is helpful to have a cursory

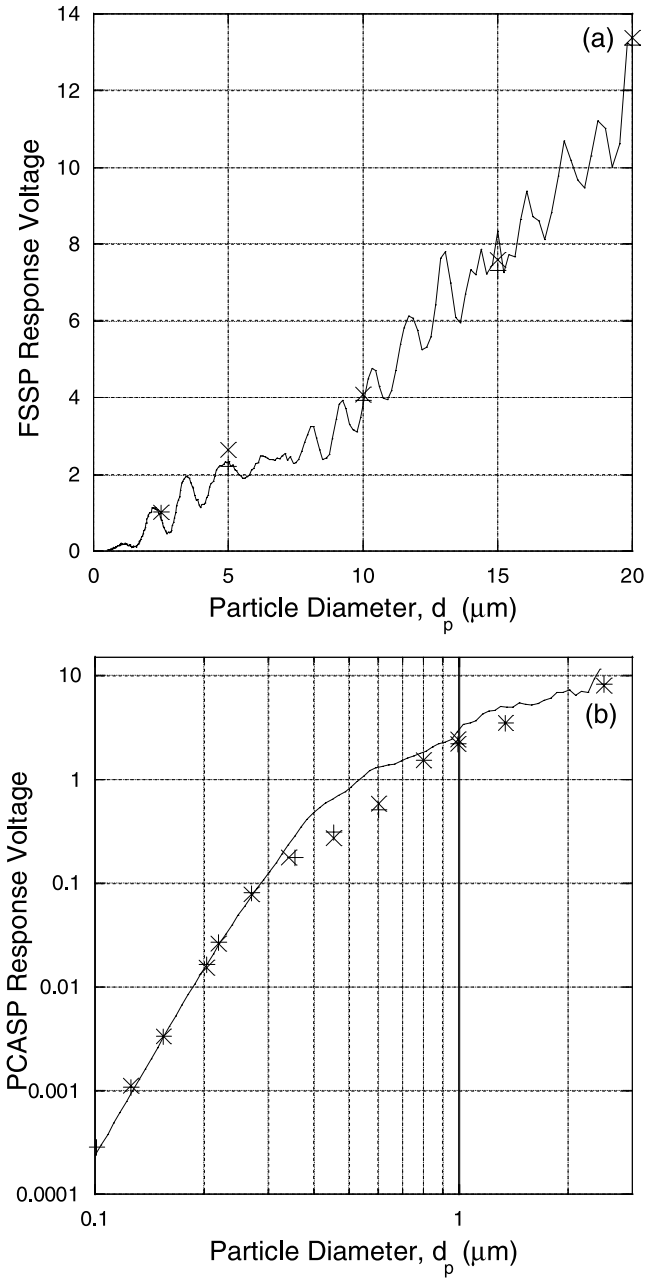

Figure 2. Calibration data for the Navajo's (a) FSSP-100 and (b) PCASP-100X using glass beads (n = 1.5) and polystyrene (n = 1.59), respectively. Solid line is the theoretical response curves. Crosses and pluses are the calibrations at the beginning and end of the mission, respectively.

examination of the dust's basic geometric properties. To this end, individual dust particles were examined using SEM techniques to evaluate their complexity as described in section 3.5. Figure 3 presents SEM micrographs of particles collected in the Saharan Air Layer (SAL) on 16 July 2000 by the Navajo. Data from this flight were typical for the study, and a complete analysis of many flights and ground samples is given by *E. A. Reid et al.* [2003].

[39] Figure 3a shows the existence of large, amorphous alumino-silicates particles transported across the north tropical Atlantic Ocean. These can be relatively large, with particles as large as 30 microns being detected on the filters [see *E. A. Reid et al.*, 2003]. In Figure 3b the much more prevalent smaller and flatter clay minerals (which had strong Al and Si X-ray features) are clearly seen [*Falkovich et al.*,

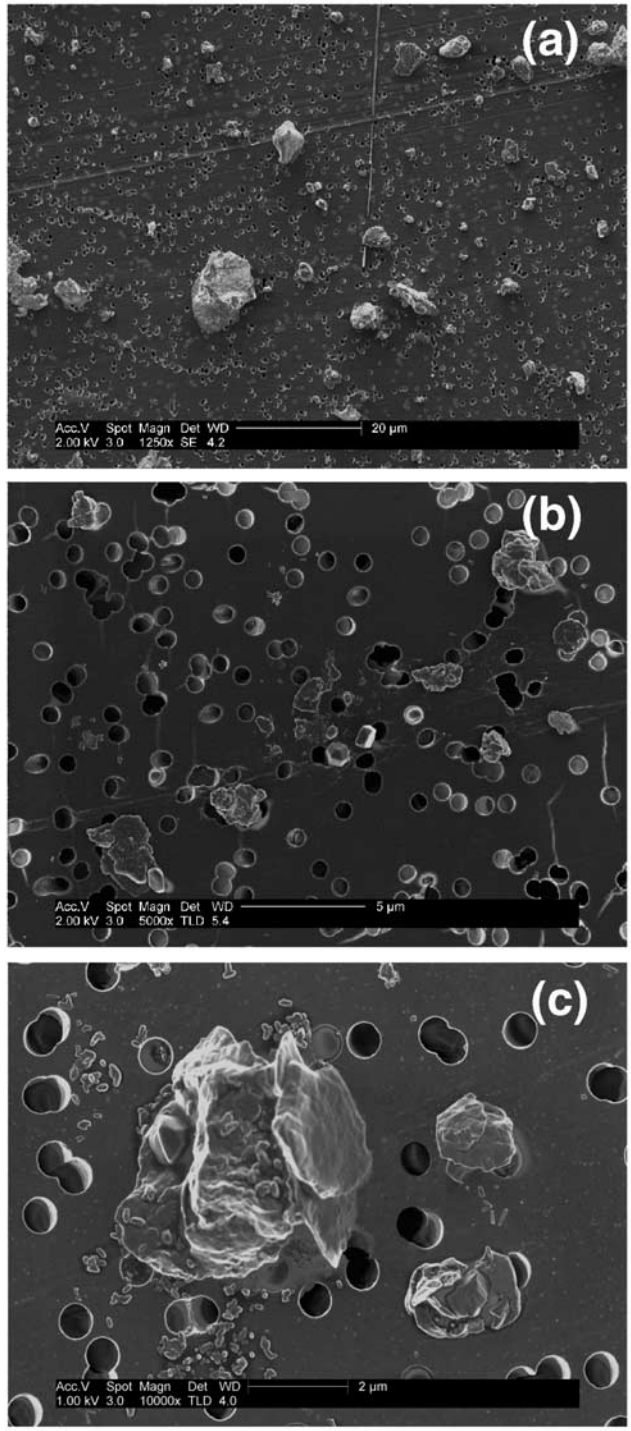

Figure 3. Scanning electron micrographs at increasing magnification of Saharan dust particles. These were collected in the Saharan Air Layer by the Navajo aircraft on 16 July 2000 on polycarbonate substrates in the vicinity of Puerto Rico.

2001; *E. A. Reid et al.*, 2003]. In Figure 3c a higher magnification is shown where clearly the complicated structure of an individual particle is shown. The remnants of aggregates that shattered on impact can be seen in the upper and lower left of the image.

[40] While images such as Figure 3 are helpful in qualitatively conveying the complicated nature of dust, some form of quantification needs to be performed. Statistics on particle geometry such as diameter of equivalent area, major and minor axes, and surface area were computed for particles with a minor axis greater than 0.75 μm. As an example, statistics generated from the 16 July SAL filter can be found in Figure 4. These statistics were generated from 17,000 particles taken on two sets of 20 × 20 contiguous images at two magnification levels from the same filter shown in Figure 3. Figure 4a presents a cumulative plot of particle aspect ratio (major to minor axis) using an ellipse best fit. This was formed automatically by the analysis software by taking the longest dimension of the particle as the major axis and constraining an orthogonal minor axis to reproduce the same cross sectional area of the particle. For this sample, the particles had a mean aspect ratio of 2.12 with a large standard deviation of 1.5 (median 2.0). This large standard deviation is related to the high degree of skewness of distribution function (∼3.5) due to the presence of a relatively low percentage of particles with aspect ratios in excess of 3 (∼8%). This distribution function did not vary significantly as a function of particle size. The mean value of 2 found here is considered typical of African dust and has found its way into spheroid light scattering computations [e.g., *Mishchenko et al.*, 1997].

[41] Normalized number and cross sectional area distributions as a function of average diameter (diameter of equivalent area) were computed and are presented in Figure 4b. Two normalized volume distributions are also presented. One is based on an ellipsoid geometry with two axes defined by the major and minor axes used above to compute the aspect ratio (recall, these axes are constrained to the cross sectional area of the particle). Since this plotted distribution is normalized to total volume, the value of the third axis to define the ellipse is not needed if one assumes that the particle depth is proportional to the particles average diameter (recall, we did not find that the particle two dimensional aspect ratio did not vary with size). A second volume estimation is presented by an extrusion method by assuming particles lay flat on the filter and that their depth is proportional to the minor axis of the two dimensional best fit ellipse. Here, the particle volumes are computed by multiplying the cross sectional area of the particle by the minor axis (again, since this is a normalized distribution we need only assume that on average the depth-minor axis relationship is independent of particle size and the actual value of the depth drops out).

[42] The particle number distribution is dominant at the smallest sizes with 90% of the particles having average diameters less than 3 μm. The area distribution had a strongly lognormal form with a median diameter of 4 μm and a geometric standard deviation of ∼2.2. The two volume distributions were also fairly lognormal and tracked similarly with a volume median diameter of 7 and 6 μm and geometric standard deviations of 2 and 2.1 for the spheroid and extruded models, respectively. The similarity of both volume estimations is expected as they derive some information from the particle cross sectional area.

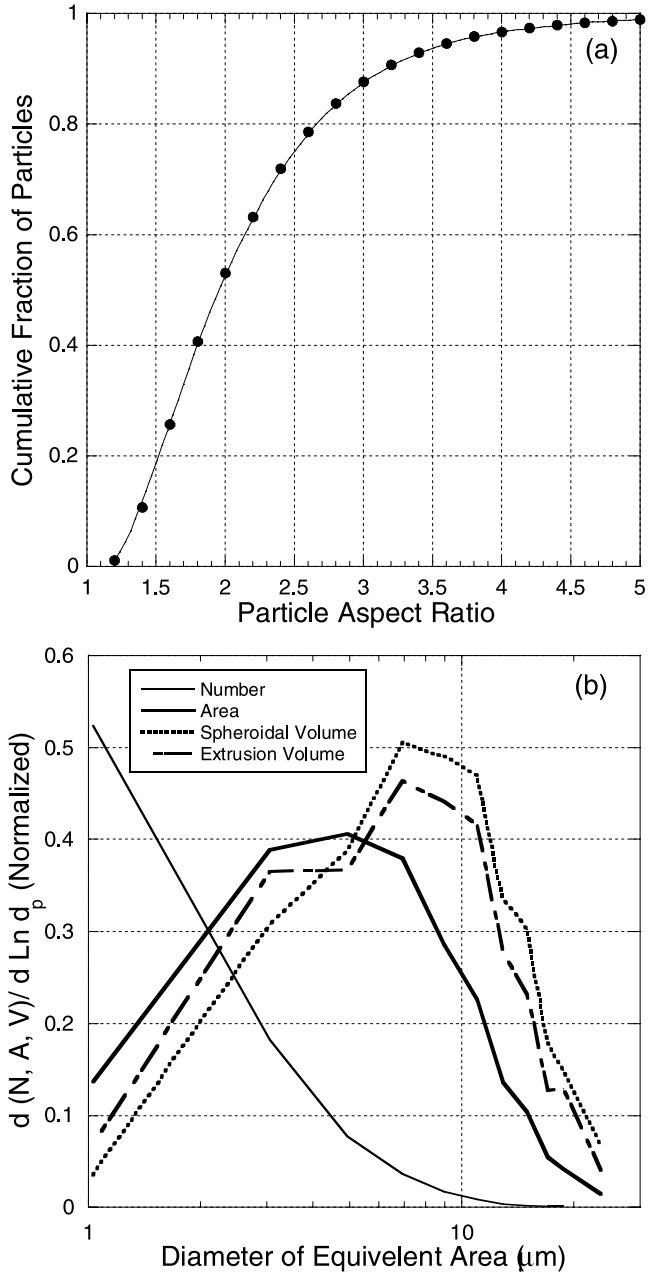

Figure 4. Plots of particle size variables for dust particles collected on 16 July 2000 based on 17,000 counted particles. (a) Cumulative plot of particle aspect ratio (major to minor axis) using a best fit ellipsoidal model. (b) Normalized dust particle size distributions of number and particle cross sectional area as a function of particle diameter of equivalent area. Also shown are volume distributions assuming an ellipsoidal model of constant mean aspect ratio with size and an extruded model (area × perimeter × depth) assuming a constant particle depth to average diameter ratio with size.

[43] Examination of Figures 3 and 4 shows the difficulty in the interpretation of geometric size distributions of dust. Qualitatively, Figure 4 shows "roughly" the size of the

particles and that they have an aspect ratio of ~1.5–3. However, geometric functions such as these do fully represent the complexity of the particles and their application to secondary products in not entirely clear. One cannot input these distributions into microphysical or radiative models as they are two-dimensional and most models cannot cope with nonspherical particles anyway. For example, the area distribution from this technique cannot be used in Mie code to calculate scattering properties as particles lay flat on the substrate and hence the area when averaged over all viewing angles would be biased high. Further while we have shown that the particle two-dimensional aspect ratio is independent of size, we cannot prove this is the case for the third dimension as was assumed in the volume calculations. In fact, as clay minerals are frequently flat plates at the smaller sizes, this third axis is likely to be on average much smaller (more than a factor of two to four) than the 2 dimensional minor axis. Hence while we can view a normalized area or volume distribution as in Figure 4b and keep its limitation in mind, we currently cannot construct a nonnormalized distribution with particle number, area and volume linked. Detailed volumetric information needs to be derived on a particle by particle basis. Estimates are made by *E. A. Reid et al.* [2003], but the uncertainties are high.

[44] Interpretation issues are compounded by a fundamental weakness of the technique; particle overlap, and aggregate particles that break up during collection. Particle overlap can be partially controlled by correctly loading a filter. In the 16 July case, only 15% of the filter surface area was covered by collected particles. Aggregates pose a more difficult issue. As large particles impact on the filter surface they can flatten and/or break apart. This results in particle sizes biasing high. This is depicted in Figure 5, where various particles in the 10 to 20 μm range are shown. In Figure 5, some solid particles are found, more than half are aggregates. As a whole, aggregates tended to be larger particles (>5 μm). These aggregates were not simply made of large clusters of particles, but often appeared to be made of only three to five large nonparticles with multiple small particles. Particles consisting of low atomic number elements appear relatively dim on the electron backscatter images, making these particle boundaries more difficult to distinguish, and the particles more likely to be missed, analyzed as several different particles, or described as unduly complex in shape. Similarly, filter topography is sometimes imaged as measured particles, and conglomerate particles are often described a multiple individual particles selected out by their brighter electron backscatter signals. It is unclear how these impacted particles and their related artifacts relate to those in the free atmosphere. Certainly, the larger aggregate particles will be more prone to this artifact. However, assessing the true impact on particle size and aspect ratio would be speculative.

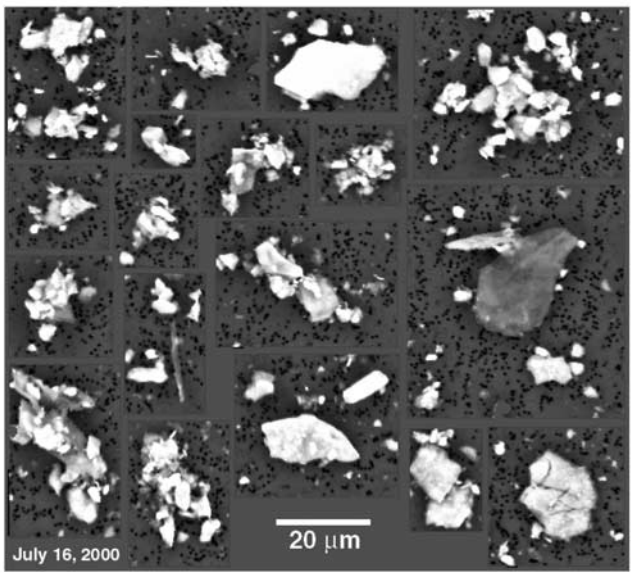

Figure 5. Mosaic of large dust particles in the ten to twenty micron range collected in the SAL for the 16 July dust event.

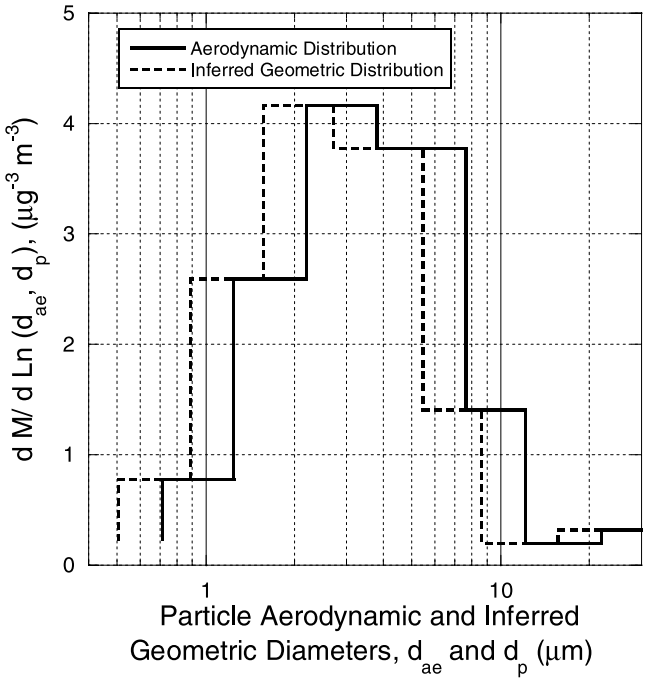

Figure 6. Mass size distribution from the ground based MOUDI impactor for the 21–24 July period. Mass was inferred from aluminum concentrations derived from neutron activation analysis.

4.2. Aerodynamic Methods

[45] During the PRIDE study Savoie et al. (submitted manuscript, 2003) submitted one integrated 70 hour MOUDI sample (21–24 July period) for neutron activation analysis. Using aluminum as a tracer species for dust they derived a dust mass-size distribution (conversion between Al and dust mass was 12.5 or 8% of mass). Both the aerodynamic and inferred geometric distributions are presented in Figure 6. The calculated dust particle aerodynamic mass median diameter (MMD) was ~3.6 μm. Similarly a lognormal curve fit of the distribution places the MMD at 3.6 μm and the geometric standard deviation of the mass distribution (σ_g) at 2 ($r^2 = 0.99$). Assuming a nominal factor of 1.4 conversion between aerodynamic and geometric diameter this infers geometric MMDs of ~2.6 μm. This MMD value is on the lower end of those presented in Table 1.

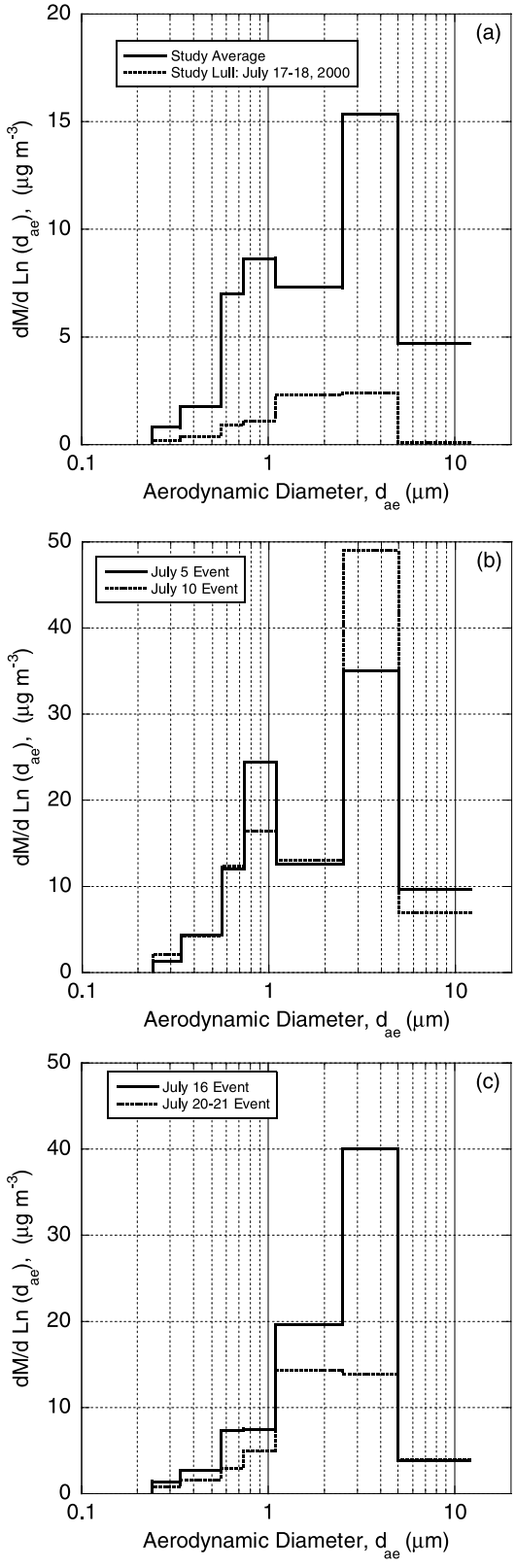

Figure 7. Reconstructed mass size distributions from the DRUM impactor as a function of aerodynamic diameter. (a) Study average (3–24 July) and the lowest dust concentration 17–18 July, (b) two early dust events (5 and 10 July), and (c) two later dust events (16 and 20–21 July).

[46] For comparison to the single event (MOUDI) we can examine the 4-hour resolution DRUM impactor data at the Cabras island site and to see if dust size distributions changed during the study. Figure 7 presents reconstructed mass size distributions using aluminum and silicon as a tracer species. Figure 7a presents the average dust size distribution for the DRUM period of operation (3–24 July, excluding 9 and 15 July), as well the 17–18 July period when dust concentrations were at their lowest. Over the study period, the most prominent size for dust related species is the "typical" saltation/transport mode in stage 2 (2.5–5 μm), suggesting best aerodynamic and geometric modes of ~4 and 2.8 μm, respectively. These values are in the middle of the aerodynamic values presented in Table 1. However, the shape of the average distribution did not fit into the lognormal model. Mass increased sharply at the stage one to two interface at 5 μm. After stage 2, the mass distribution lowers and flattens for the next 3 stages. There is even an additional small mode in stage 4 at ~0.9 μm. These aspects of the distribution result in calculated MMD of 2.7 μm (~1.9 μm geometric) or roughly a micron less than the MOUDI sample of 21 July.

[47] The dynamics of the dust size distribution can be seen in Figures 7b and 7c, where reconstructed mass distributions are displayed for the four other dustiest events captured by the DRUM (5, 10, 16, and 20–21 July). Here, the DRUM sampler showed some systematic shifts in the distribution. Systematically through the field study, the DRUM transitioned from very sharp peaks in stage 2 and 4, to a generally smoothed single mode distribution by 16 July. While these shifts in the size distribution were occurring, there was no systematic shift in the computed MMD; the MMD varied between 2.8, 3.1, 2.8, and 2.3 μm for the 5, 10, 16, and 20–21 July cases. Further, the shift in the DRUM mass distribution shape did not correlate with dust concentration or in changes in bulk dust chemistry. The only systematic difference we found was that as the field study progressed, SAL dust layer transport developed and the relative amount of dust in the marine boundary layer decreased relative to that aloft [*J. S. Reid et al.*, 2003].

[48] To check for consistency, we can plot the aluminum mass distribution for the MOUDI and DRUM sampler during the 21–24 July sample period. These two instruments are plotted against each other in Figure 8. During this time period, the total integrated Al concentration for the two samplers was nearly the same (0.63 ± 0.03 and 0.70 ± 0.1 μg m^{-3} for the MOUDI and DRUM, respectively). However, systematically there are differences. Despite the larger modal diameter of the raw impactor data (3.5 versus 3 μm for the DRUM and MOUDI, respectively), both the calculated and best fit MMDs have the DRUM samples systematically smaller than the MOUDI by 1 μm. The DRUM distribution is also considerably wider with geometric standard deviation of 2.4, versus only 2.0 for the MOUDI.

[49] Finally, the mass distributions from the two impactors can be compared to the TSI aerodynamic particle sizer (APS) colocated at the University of Miami mobile laboratory. Recall, unlike the impactors which measure integrated mass as a function of aerodynamic diameter, the APS is a single particle counter measuring number as a function of aerodynamic diameter. On the basis of a regression analysis of particle size from the APS 3310 and sea salt and dust

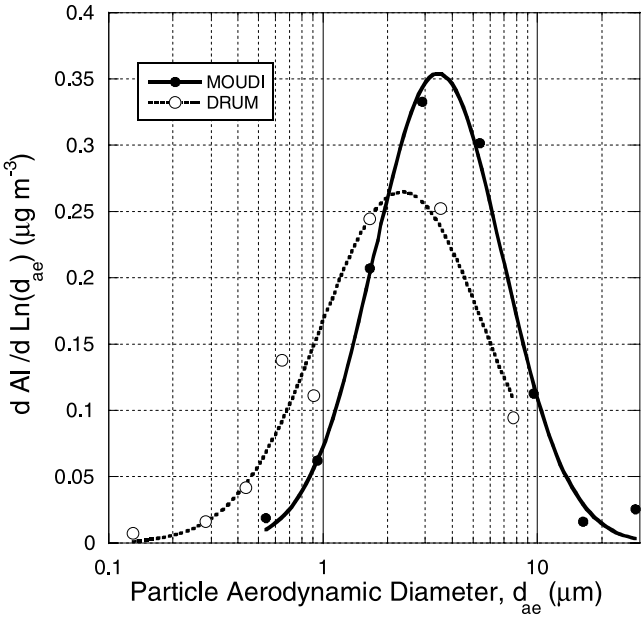

Figure 8. Average aluminum mass distributions from the MOUDI (solid circles) and DRUM (open circles) impactors in coincident time between 21 and 24 July. Lognormal curve fits are shown (MOUDI solid line, DRUM dotted line). Despite the difference in modeled mass median diameter (3.4 μm versus 2.3 μm for the MOUDI and DRUM, respectively) and geometric standard deviation (2.0 versus 2.4 μm for the MOUDI and DRUM, respectively), the two instruments measured the same bulk mass concentration of 0.6 μg m^{-3}. Both should be considered good fits with $r^2 > 0.94$.

concentrations from the bulk filter measurements, *Maring et al.* [2003a] derived a mean dust aerodynamic volume distributions averaged over PRIDE field study. As in previous studies, for PRIDE using an effective density of 2 g cm^{-3} yields the same mass concentrations as the filters and TEOM. Hence an inferred geometric volume distribution was also generated again using the factor of 1.4 between aerodynamic and geometric diameter. These aerodynamic and inferred geometric dust distributions are presented in Figure 9 along with lognormal best fits.

[50] The APS gave a volume distribution considerably larger than the impactor samples. The APS shows two weak modes at 5 and 9 μm, and 3.6 and 6.5 μm for aerodynamic and inferred geometric diameters, respectively. Like the DRUM sampler, this distribution was not strongly lognormal. The calculated aerodynamic volume median diameter based on the APS spectrum yields a value of 5 μm (3.6 μm geometric diameter). An unsupervised lognormal curve fit of this distribution places the VMD at the same value as the direct calculation (aerodynamic VMD = 5, $\sigma_{gv} = 2.2$, $r^2 = 0.8$), but this is done by reducing the variance around the first mode and smaller particles. As can be seen in Figure 9, the lognormal distribution does not represent the larger particles particularly well. Particles in the 8–12 μm range are underrepresented relative to those larger than 12 μm. Going to a bimodal representation gives a better fit, but requires a second lognormal distribution centered on 9 μm with an unphysically low σ_{gv} of 1.15.

[51] All three of the aerodynamic methods give fairly reasonable values relative to other aerodynamic methods listed in Table 1. However, even though collocated, clearly significant differences do exist between the methods. From all of the available data from the study, one would get an aerodynamic MMD of 2.7, 3.6, and 5 μm for the DRUM, MOUDI, and APS 3310, respectively. Again assuming a simple empirical factor of 1.4 conversion between aerodynamic and geometric diameter, this corresponds to geometric MMDs of 1.9, 2.6, and 3.6 μm. Taken at face value when compared to the mass extinction calculations in Figure 1a, this would imply almost a factor of two variance in calculated mass extinction efficiencies from the three distributions. Can these differences be reconciled?

[52] First, let us consider the impactors. There are two significant issues that would cause a smaller size distribution to be found in these sampling systems: inlet losses and particle bounce/breakup. There is strong evidence that inlet issues are an important factor for the PRIDE case. Both impactors measured nearly the same aluminum mass concentration, suggesting that analytically the two systems are comparable. However, comparison of the reconstructed mass of these instruments using aluminum as a tracer is a factor of 1.6 lower than coincident bulk filter measurements and the TEOM. For example, over the 21–24 July period,

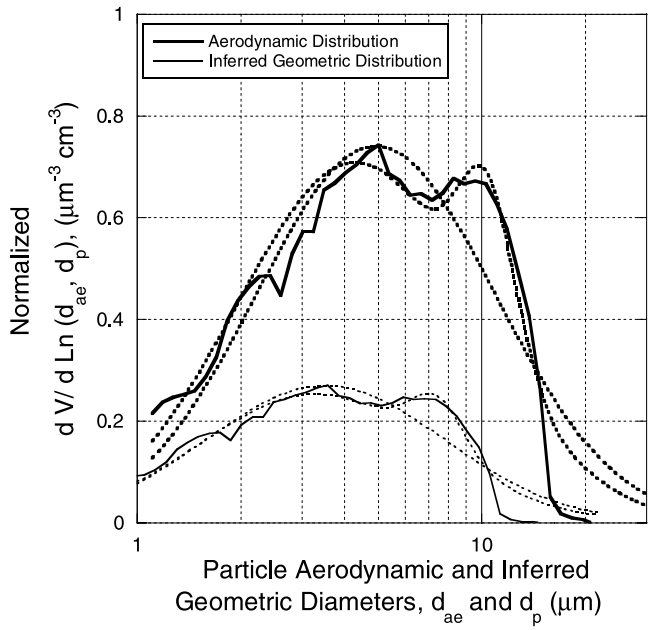

Figure 9. Normalized PRIDE study-averaged dust distributions derived from the ground based aerodynamic particle sizer (model 33). Shown are volume distributions computed from the aerodynamic (thick lines) and inferred geometric (thin lines) diameter. Also shown are the single log normal curve fits (VMD = 4.9 and 3.5, geometric standard deviation = 2.2 and 2.2 for the aerodynamic and inferred geometric distributions respectively) and bimodal curve fits (aerodynamic VMD of 4.5 and 10.4 μm and geometric standard deviation of 2.2 and 1.15; Geometric VMD of 3.3 and 7.4 μm and geometric standard deviation of 2.2 and 1.16). There is a factor of 2.7 difference in volume between the aerodynamic and geometric distributions.

bulk filter samples give an estimated dust mass concentration of 16 $\mu g\ m^{-3}$ by an ashing technique compared to 7.8 and 8.4 $\mu g\ m^{-3}$ for the MOUDI and DRUM impactors, respectively (using a factor of 12.5 aluminum to mass ratio or 8% of total mass). We are confident in this aluminum to mass ratio as it has been found in analytical soil studies [*Taylor and McLennan*, 1995], previous mass closure experiments [*Maring et al.*, 2000], and fits with the stoichiometry of the particles [*E. A. Reid et al.*, 2003]. This suggests that half of the particle mass was not penetrating the inlet. The TEOM and APS samples shared a common capped inlet operating at 300 L per minute (Lpm). The bulk filter had its own inlet but sampled at 300 Lpm. At the typical 7 $m\ s^{-1}$ wind speeds, there would be no difficulty in sampling particles as large as 20 μm. The DRUM impactor sampled off of its own capped inlet at only 10 Lpm, and the MOUDI sampled from its own inverted "U" inlet at 30 Lpm. It is unclear what the intrinsic cut points of these inlets are. Sampling at only 10 Lpm, the DRUM sampler may not have the drawing power to pull particles larger than 6 microns. This would explain the very sharp increase in particle mass from stage 1 to 2. Similarly, it has recently been found that the "U" inlet design may drastically under sample large particles. From unpublished data during the recent Atmospheric Characterization Experiment-Asia (ACE Asia), a MOUDI sampler using the same inlet design at Che Chu Island found 100% penetration for nonmicrometer sulfates, but underestimated dust concentrations by more than 50%.

[53] Aside from the inlet issues, we must return to the fact that the MOUDI and DRUM substrates measured the same amount of aluminum. Why are there differences in distribution shapes for the two methods? In most intercomparison studies, these differences could probably be considered fairly good as there are differences in the channel widths, cut-point sharpness, and calibration factors between the two methods. Further, there is an inherent uncertainty in fitting wide binned data such as those from impactors. However, the DRUM sampler does consistently show higher particle concentrations at the smaller sizes. It is possible that this difference is a result of particle bounce/fragmentation.

[54] All inertial impactor methods must cope with the issue of bounce. Bounce occurs when a particle, which should stick to a particular substrate, bounces off and gets collected on subsequent stages or an after filter. Typically the collection substrates are coated with sticky substances so this does not occur unless substrates become heavily loaded. However, in the case of aggregates (such as the dust particles shown in Figure 5), the primary particle may shed some smaller particles on impact that never touch the actual substrate. These smaller particles would then be collected on subsequent stages. We hypothesize that in the case of the DRUM sampler, this effect would be exaggerated. Consider that before the stage of the MOUDI containing the dust mass mode (cut point of 2.2 μm,) a particle must traverse 4 additional stages (22, 12.1, 7.6 and 3.6 μm). Larger particles will impact on these earlier stages at relatively low velocities and the probability of shedding is small. In the case of the DRUM sampler, however, the first cut point in stage 1 is at 5 μm. Any large dust aggregates penetrating the inlet will hit this stage at a relatively high velocity and perhaps shatter on impact. Individual secondary particles would then cascade through the system. The resulting size distribution for this scenario would probably match that found on the DRUM with a large peak in stage 2 and a gradual drop off to smaller sizes. Hence the secondary 1 μm mode found in the DRUM sampler in the early half of the study (e.g., Figure 7b) may be due to the presence of relatively few large dust particles that are transported under those flow conditions.

[55] The difference between the impactors and the APS is more complicated. Certainly the VMD for the *Maring et al.* [2003a] mean APS distribution and the mean MMD from the MOUDI impactor compare very well (this is remarkable as it is probable the MOUDI is under-sampling larger particles). However, structurally there are differences with the APS being bimodal with a significant amount of volume at larger sizes. A significant difference between the two methods likely exists because ultimately the impactors make mass measurements and the APS makes number measurement. This distinction becomes more important as particles become more heterogeneous in shape and density. In the case of large aggregates in particular, one does not have to worry about particle deformation and shattering on a surface like in the DRUM impactor as the APS sizing is performed in an air stream.

[56] If the APS bins particles in a size larger than that of an impactor, it may imply that most of the particles have a high drag to mass ratio (as expected; see Figure 3). More simply, more of the mass is associated with particles with high drag coefficients (e.g., plate-like clay minerals). Compounding this, as a particle becomes more irregular, the surface area (and hence drag) to volume ratio must increase. Given that χ values are on the order of 1.2 to 1.8 for differing dust particles, the APS will be more likely to give a wider size distribution. This distribution should become wider as particles become more asymmetric or elongated. The factor of 1.4 we use between aerodynamic and geometric diameter is an average and varies from particle to particle. Since the APS distribution is bimodal, it may be separating individual dust species with characteristic drag to mass ratios and morphologies such as clays and silicates.

[57] There are also some calibration issues related to the APS that merit discussion. Calibration studies have suggested that the APS undersizes particles with irregular shapes such as dust [*Marshall et al.*, 1991]. Because particles flow through the APS at super-Stokesian velocities, irregular particles can deviate from the velocity to particle size calibration curve in unpredictable ways. *Marshall et al.* [1991] suggested the APS could undersize particles by 25% for dynamic shape factor (χ) values of 1.2 (recall, dust as χ values of 1.2–2). Thus, while variance in the drag-mass ratio can cause variations in the APS size spectra, one must still be cautious when relating these differences to true aerodynamic diameter. Regardless, these findings would suggest that the true difference between the APS and the impactors may in fact be greater than what is shown in the figures and/or that there is a cancellation of errors from other sources, such as the computation of volume from single particle counts.

4.3. Airborne Forward Scattering Spectrometer Probe

4.3.1. PMS Probe Data

[58] In the previous sections, we discussed particle sizing from geometric and aerodynamic methods. In this section we scrutinize the response of optical particle counters to

dust particles by examining the Forward Scattering Spectrometer Probe (FSSP) data collected near the Cabras Island site. Size distribution measurements from the Navajo's PMS probes were performed during a vertical profile over the site on each flight. Particle number, surface area, and volume distributions for the PMS probes are given in Figures 10a, 10b, and 10c, respectively. These size distributions were taken in the middle 1000 meters of the dry Saharan Air Layer for 5 significant dust events of 28 June and 5, 10, 15, and 21 July (a complete description of these events are given by *J. S. Reid et al.* [2003]).

[59] Over the entire study period, such size distribution plots of PMS probe data did not indicate any significant change in the coarse dust size. Examination of Figure 10 shows that almost every peak, inflection, and trough in the distribution shape is reproduced for each day. Only the relative magnitudes are shifting. From the number distributions, it appears that the count median diameter is in the 1–2 μm range. Volume median diameter and distribution modes are at 9–10 μm with an average geometric standard deviation of 1.6. Similarly, the surface area modal diameter is also at 9 μm but the surface area mean diameter is somewhat smaller at 7 μm, a characteristic unlike lognormal distributions.

[60] The relative differences between the PCASP and FSSP in the overlap region (~1–3 μm) were also static in the SAL throughout the study. Between FSSP channel 1 and 2 (1–1.7 μm) the PCASP and FSSP cross over. In the FSSP channel 2 to 3 range (1.7 to 2.5 μm), the FSSP showed concentrations consistently a factor of 2.2 ± 0.2 higher than the PCASP.

[61] The characteristic shape of the distribution function of data from the FSSP also did not significantly vary as a function of altitude. Throughout the study, size distributions of dust in the MBL did not differ significantly from dust in the SAL. Figure 11a shows the atmospheric sounding and vertical profile of the particle surface area concentration for the 28 June dust event at Cabras Island. As discussed by *J. S. Reid et al.* [2003], the 28 June event had some of the highest dust concentrations during the PRIDE study, and was a good example of how dust transport in the Caribbean region is not always aloft in the Saharan Air Layer. On this day, a scattered tropical cumulus layer was present at the marine boundary layer/trade inversion at ~1100 m. For this event there was more dust in the marine boundary layer than above in the SAL. It was estimated that 75% of the coarse mode mass in the MBL was from dust [*Reid et al.*, 2002].

[62] Figure 11b shows the measured surface area distributions for the MBL (RH = 68%), at clear air around cloud base (RH = 85%), and in the SAL layer (RH < 40%). As in all of the SAL cases in Figure 10, the surface area modal diameter is at 10 μm, and only the relative magnitude of the FSSP distribution is shifting in the 4 to 15 μm range. As in all cases during PRIDE, at higher relative humidity (e.g., at cloud base) particle surface and volume concentrations increased significantly (note the peak in concentration in Figure 11a at the MBL/trade inversion). If particle concentrations are amplified at cloud base, one would expect salt droplet growth to be the causal factor. However, these increases were not reflected in any apparent change of size in the distribution, only the magnitude.

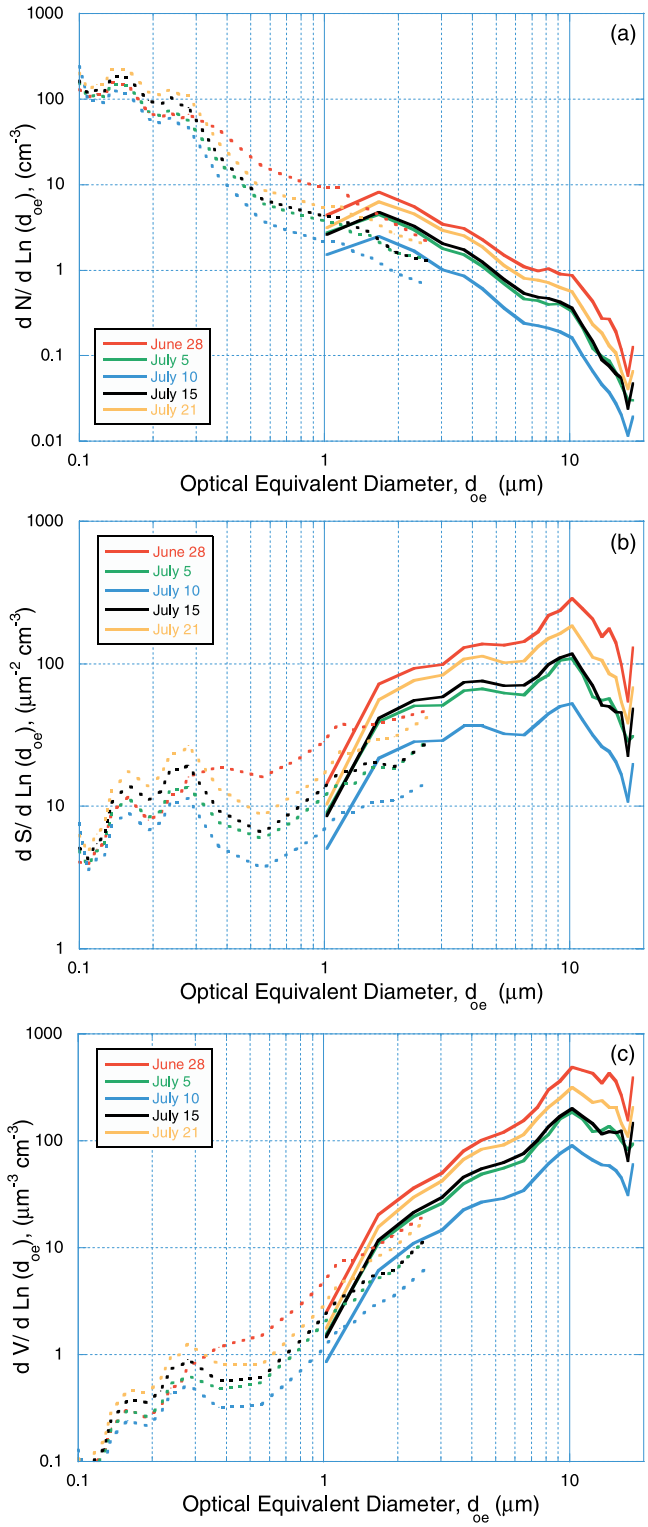

Figure 10. Combined PCASP (dashed lines) and FSSP-100 (solid lines) particle size spectra taken in the SAL for five dust events (28 June and 5, 10, 15, and 21 July). (a) Number distribution, (b) surface area distribution, and (c) volume distribution.

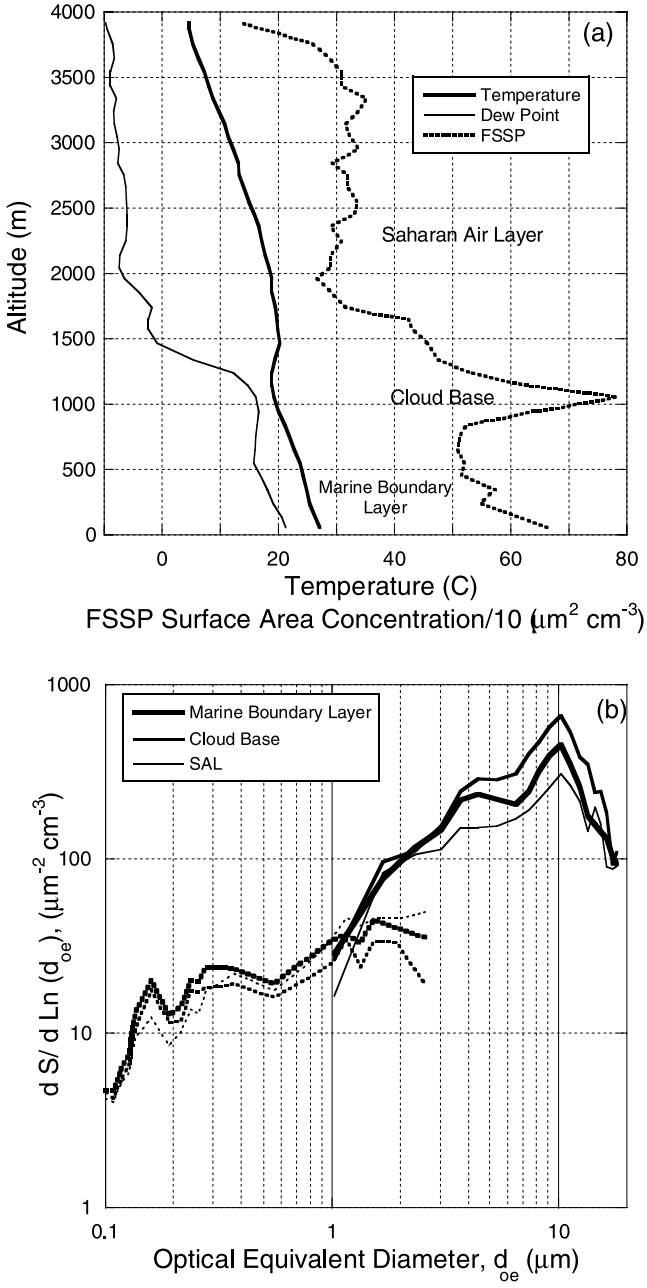

Figure 11. Thermodynamic and particle soundings for 28 June 2000. (a) Temperature and dew point (thick and thin lines, respectively) and particle surface area concentration from the FSSP. (b) PCASP and FSSP surface area distributions for the marine boundary layer (thick line), cloud base (medium line), and Saharan Air Layer (thin line). FSSP is in solid lines, and PCASP is in dotted lines.

[63] Although there was no shift in FSSP distribution size, one shift as a function of height was apparent. In the PCASP-FSSP overlap region we did find a strong sensitivity to relative humidity. As discussed in relation to Figure 10, in the dry SAL region (RH < 40%) the difference between the PCASP and FSSP in the overlap region was a fairly static factor of 2.2. In Figure 11b we find that the difference between PCASP and FSSP becomes greatest in clear air regions around cloud base height, where they differ by more than a factor of 4. In the MBL (RH = 75%), we find a factor of 3 difference. As the PCASP and FSSP measure dry and ambient size distributions, respectively, this increased difference may be due to the growth of sea salt into the FSSP sizing range. While this would describe an increased discrepancy, one must note that the increased difference is not due to an increase in the FSSP but rather a falloff of the PCASP. Hence this difference may also be due to inlet nozzle losses of more hydrated droplets in the PCASP.

4.3.2. Comparison of Data to Mass and Aerodynamic Measurements

[64] Comparison of the size distributions from the airborne PCASP and FSSP probes to those from aerodynamic methods for the PRIDE field study show the same differences as seen in Table 1; a characteristic volume median diameter of 9 μm was found, compared to the VMD's of the aerodynamic methods of ~4 μm. This can in part be explained from data from Navajo flybys of the University of Miami aerosol sampling trailer at Cabras Island. Figure 12a displays the comparison of the total number of particles measured by the FSSP and the ground base APS in the 1 to 20 μm range. Here we find a very good comparison with a slope of 1.15 and an r^2 value of 0.83. Differences on most dust days are only 10%. Hence the FSSP and the APS are measuring the same number of coarse mode particles (The Y axis offset is explained by the fact that the APS measures dry size distributions and the FSSP measures size at ambient relative humidity. This shift is due to the presence of hydrated salt particles counted by the FSSP.).

[65] A comparison of the FSSP total volume concentration to the surface based TEOM mass (Figure 12b) is also linear. Shown in a regression line forced through zero yielding a slope of 0.16 ($\mu g\ m^{-3}$) ($\mu m^{-3}\ cm^{-3}$)$^{-1}$ and an r^2 of 0.63 (If we allow for a Y intercept, the regression slope reduces to 0.13 with a nearly identical r^2 of 0.65). One point may be an outlier, but is included in the regression shown. Its removal would increase the slope to 0.18 ($\mu g\ m^{-3}$) ($\mu g^{-3}\ cm^{-3}$)$^{-1}$ a r^2 of 0.75 and the best fit would go through zero. Hence we consider this correlation fairly good with roughly a slope of 0.16 ± 0.02 ($\mu g\ m^{-3}$) ($\mu g^{-3}\ cm^{-3}$)$^{-1}$. So, assuming an effective dust density of ~2 g cm^{-3} the FSSP measured a volume concentration a factor of 12.5 too high. Hence, while the comparison with the APS shows that the FSSP was counting the correct number of particles the TEOM data suggests that the FSSP is oversizing dust particles by an average of ~2.3!

4.3.3. FSSP Oversizing Issues

[66] This issue of over sizing is explainable when one considers the engineering behind the FSSP. All optical particle counters (OPCs) are based on the principle of relating the amount of light scattered off a particle from a white light or laser beam into a detector to that of some standard sphere of known size and index of refraction. Simply put, OPCs measure pulse heights in a detector and relate that pulse height to some empirical curve fit using standard spheres. Almost all investigators correct these calibration curves to account for the mean index of refraction of the aerosol particle type being measured. For fine mode particles such as measured in the PCASP, this is a straightforward calculation. Further, the response of scattered light to size is so strong for small particles that small

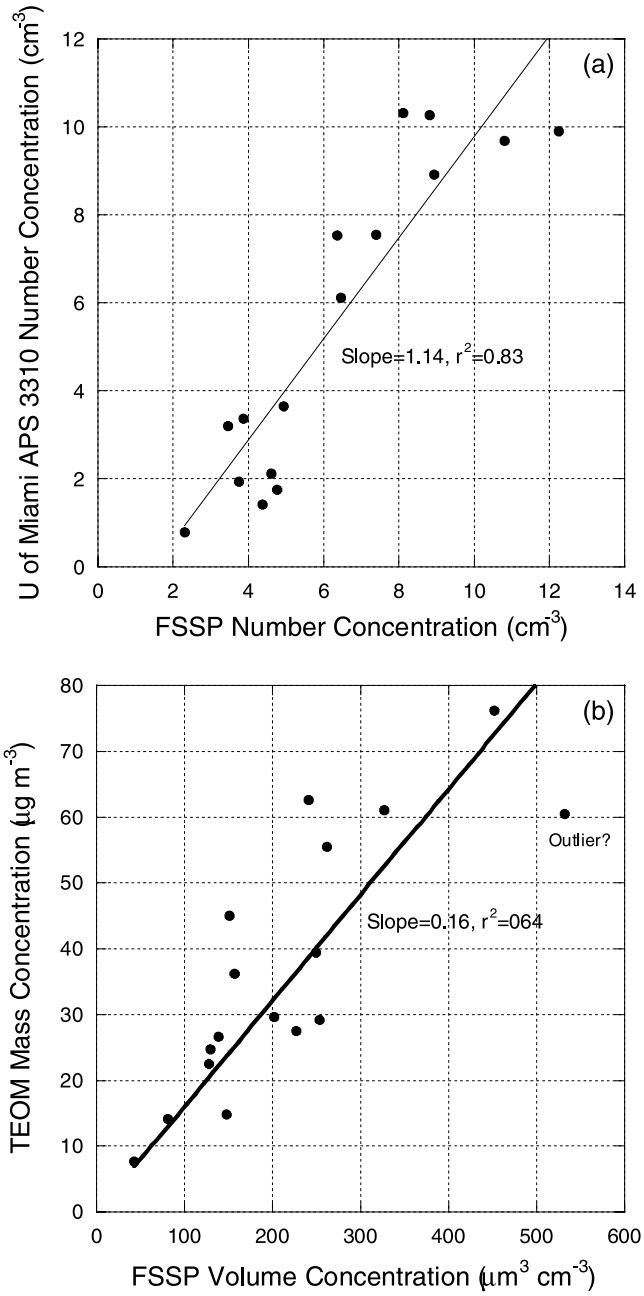

Figure 12. Comparisons of (a) FSSP and APS number concentrations and (b) FSSP volume and TEOM mass concentrations for all 17 occasions when the Navajo flew by Cabras Island site when the surface instrumentation was operational.

perturbations in index of refraction can cause small uniform size shifts, but not disrupt the shape of the particle distribution function. However, as discussed by *Collins et al.* [2000], the FSSP-100 in particular is insensitive to particle size in the ~3 to 10 μm range. This is due to frequent Mie oscillations and compounded by an inflection point at 5 μm in the Mie size-scattering cross section curves at the FSSP scattering angles (~4–12°). The presence of this inflection point can be seen in the FSSP calibration shown in Figure 2a. Clearly, the relationship between particle size and scattered light into the FSSP detector is not one-to-one for particle sizes where dust exists.

[67] The striking difference between the FSSP and aerodynamic methods in the PRIDE case relates to the properties of dust, particularly to variability in particle index of refraction and shape. All aerosol species are somewhat heterogeneous in nature, being a combination of internal and external mixing and hence there is some distribution of index of refraction. For airborne dust this heterogeneity can be extreme-there are multitudes of minerals with strongly varying indices of refraction. For example, clay minerals (such as illite and kaolinite) which are dominant minerals in dust transported into the Caribbean have an index of refraction in the range of ~1.54–1.63 with a mean around 1.57. Also present are minerals such as feldspars and micas with varying real part indices of refraction from 1.5 to 1.6, and carbonates and silicates up to 1.68. Further, for individual minerals the index of refraction even varies by particle axis. In the marine boundary layer, one must also account for hydrated sea-salt particles with an index of refraction of <1.4. The impact of varying index of refraction on the FSSP response function can be seen in Figure 13a. Here, theoretical response curves for 4 indices of refraction are presented n = 1.33 (water), 1.5, 1.6, and 1.7. As we allow for variability in the index of refraction on a particle per particle basis, it becomes quite clear how large a sizing uncertainty there is. For water droplets (n = 1.33) for which the FSSP was originally intended, the response curve is fairly steep. However, for index of refraction values common to dust, the response lessens. Given that the response curve used for this study is a smoothed form of the n = 1.5 curve, a particle scattering a 2.5 volt pulse height could really be anything from a 4 to 9 μm particle.

[68] Compounding the situation with index of refraction are the particle morphological considerations (e.g., see Figures 3 and 5). Dust particles are made up of flat clay minerals, cylinders, and polygonal aggregates. As each dust particle passes through the sampling volume of the FSSP, each will scatter light into the 4–12° scattering angle detector differently based on their random orientation geometry. A flat clay mineral can pass through showing a maximum facial area to the beam and be "oversized", or it can pass through with the thinnest side and be undersized. Hence the resulting size distribution will have considerable broadening to account for the various particle morphologies. As particle number concentration naturally falls off with size, even if as few as one-in-three 5 μm particles is oversized to 9 or 10 μm, this is enough to skew this distribution.

[69] Dust particle phase function must also be considered. *Mischenko et al.* [1997] showed that the phase function of spheroids when averaged over all orientations was insensitive to particle asphericity in the forward scattering angles. In the FSSP scattering range the average phase function for averaged spheroids representative of dust has an increased phase function of ~5%. However, they also found that a single spheroidal shape has a unique phase function unlike any other, probably adding another 15% uncertainty. When one considers that dust is not even accurately portrayed by spheroids, the uncertainty on a particle to particle basis is even greater. *Collins et al.* [2000] showed using the phase functions of *Mishchenko et al.* [1997] that for FSSP

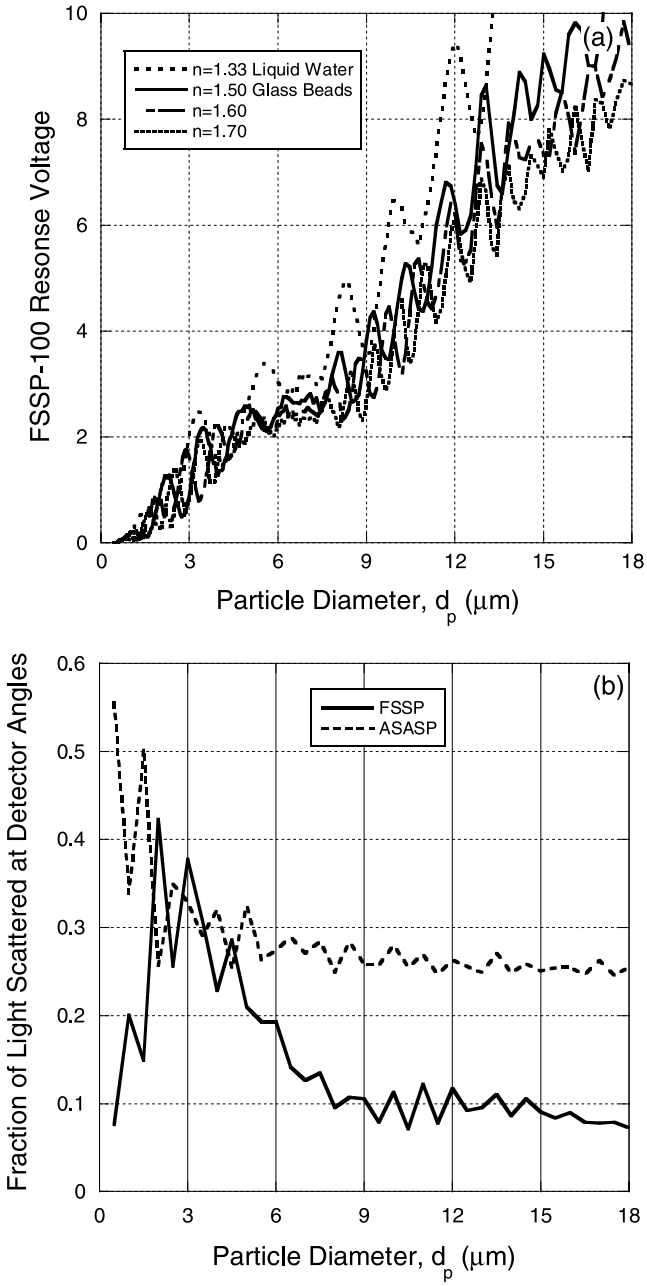

Figure 13. (a) FSSP response function for spherical particles for four refractive indices. (b) Relative fraction of light scattered at detector viewing angles for the FSSP and ASASP instruments assuming spherical particles and an index of refraction of 1.5.

scattering angles, the ratio of spheroid to sphere scattering for dust-like spheroids was only about 1.06 (or 6% increase). However, recent work of *Kalashnikova and Sokolik* [2002] has shown that if more realistic particle shapes are used, then dust particle phase functions in the FSSP viewing range can be as much 20% higher. Given the uncertainty in the response curve, even small deviations can have an impact on size and hence derived higher moment distributions. In conjunction with the flatting in the FSSP response curve shown in Figure 13a, such an increase would cause a gross overestimation of particle size and hence surface area.

[70] It has been suggested at recent scientific meetings that the sampling volume of the FSSP is in error. As discussed above, the FSSP is measuring twice as many particles as the PCASP in the overlap region. If there is an error in the computation of the FSSP sampling volume and we compensate by adjusting the FSSP sampling volume such that these two probes align, then the number concentration in the FSSP would decrease by a factor of two. The problem with this solution is that as is shown in Figure 12 the FSSP is counting the correct number of particles. Further, the volume is overestimated by more than an order of magnitude, not just a factor of 2.

4.3.4. Utility of FSSP Data

[71] The strong differences between the PMS probe size distribution and those of the aerodynamic methods, as well as the somewhat unusual behavior of the PMS sizing as a function of altitude makes one question the usability of the data. As shown in Figure 1, a shift in VMD from 4 to 9 μm is enough to drop the mass extinction efficiency of dust by more than a factor of 2. Include the volume overestimation and calculations of a factor of 12 and the uncertainties are indeed large. This is certainly troublesome when one considers all of the studies based on optical measurements of dust particles (Table 1). However, examination of the data shows that when used in the correct context the PMS probes can still be useful in analyzing and interpreting dust data sets.

[72] Fundamentally, the FSSP is a particle counter and hence can accurately give the number concentration of coarse mode particles. Relative fine mode/coarse mode partitions can be determined. Most of the issues relating to the FSSP are in regard to higher moment distributions (i.e., due to distribution widening and individual particle over sizing). However, there should still be information in the number distribution. During PRIDE, the FSSP had a number mode in channel 2 (~1.8 μm). Typically, the first and last channel of any optical particle counter are ignored. Hence one cannot clearly say FSSP channel 2 contains the number mode. However, from Figure 10 it is clear that there is a flattening of the number distribution in the 1 to 2 μm range (probably the location of the mode). There are other "flattened" portions of the spectrum in the 4 to 7 μm and 8–11 μm ranges where particles are indistinguishable by the instrument. These portions of the size spectrum are as close to independent channels as can be derived with the FSSP. By comparing the ratio of counts in these various regions of the curve, shifts in the particle size distribution as a function of altitude become more visible. Figure 14 shows the vertical profile of the ratios between these three ranges for the 28 June case shown in Figure 11. Here it is more evident that there is a shift in particle size at the marine boundary layer, with the ratio of 2 to 5 and 9 μm particles increasing by a factor of 2. A larger falloff is even more pronounced at the top of the SAL layer. This ratio between the 2 and 5 μm particles is consistent in the data set with particles in the 1–3 μm range best displaying shift in dust particle size with altitude. In contrast, there is no shift in the ratio of 5 to 9 μm particles suggesting that there is no variance in particle size between these two sizes (likely through cross contamination). Hence, while the display of a distribution function is not as useful in conveying shifts in particle properties with the FSSP, ratios can display some qualitative information on particle vertical distribution.

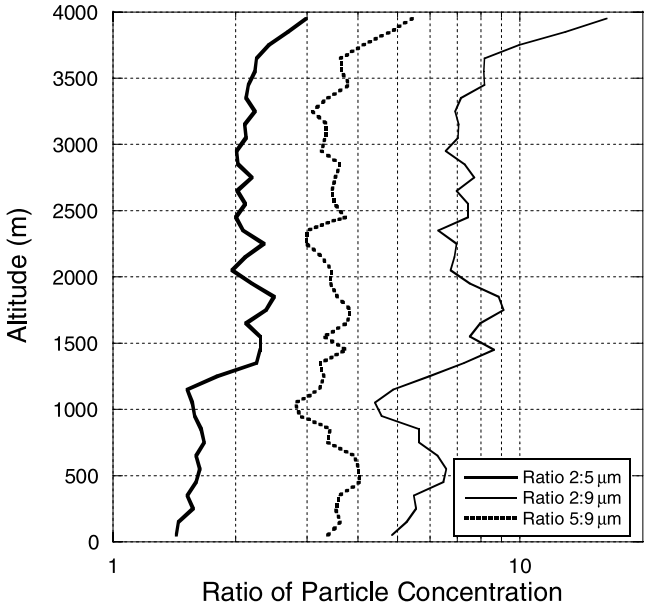

Figure 14. Ratio of particle concentrations for the 28 June case shown in Figure 12. Curves are for the ratio of 2 to 5 μm (thick solid line) and 2 to 9 μm (thin solid line) and 5 to 9 μm (dotted line) particles.

[73] A second point to be mindful of is that regardless of sizing issues the FSSP is measuring scattering pulse heights. Hence we would expect that the ensemble cross sectional surface area of particles measured by the FSSP should be correlated to the particle scattering coefficient. This is demonstrated in Figure 15a where the column integrated FSSP cross sectional surface area is compared to the column optical depth measured by the airborne Sun photometer on the Navajo for 20 profiles when sky conditions permitted the comparison. Over the vertical profile column, the relationship is extremely strong, with a r^2 value of over 0.95. This r^2 is maintained whether the regression is against FSSP number or volume distributions as well. Because no PCASP data goes into this regression, it demonstrates the dominance of dust in the atmosphere, as we have not accounted for the influence of any uncorrelated fine mode particles. This relationship also holds for specific portions of the atmosphere. In Figure 15b, the regression is made for only the SAL layer, the convective boundary layer (CBL), and the marine boundary layer (MBL). In each case, the regression line is the same. Further, while the regression becomes noisier in the CBL and MBL, one must consider that the differential optical depths are smaller for these regions, and to derive a data point one must assume that the optical depth above is remaining constant. This regression implies that to convert FSSP surface area concentration (in $\mu m^2\ cm^{-3}$) to extinction (in Mm^{-1}) for this study, the value need only be multiplied by 0.33 $cm^2\ cm^{-2}$. This can be then applied to get higher resolution light extinction profiles in the atmosphere. Examples of these are given by *Livingston et al.* [2003].

[74] From the above demonstrations, the FSSP shows its utility in qualitative ways. However, is there an easy interpretation for what the FSSP is measuring aside from "large particle condensation nucleus counter" and "forward scattering nephelometer," or is there a way to correct or invert the data to some quantity more usable to scientists? There have been several attempts to correct the data. We discuss these below.

[75] *Collins et al.* [2000] suggested that for African dust measured in ACE-2 the FSSP size bins in the coarse aerosol region be reduced to only three in the $d_{oe} < 10$ μm range- <1.5 μm, 1.5–4 μm and 4–8 μm. However, the volume distribution plots of *Collins et al.* [2000] showed the area and volume continuing to increase past the 8 μm range; hence the same volume distribution is derived as we found

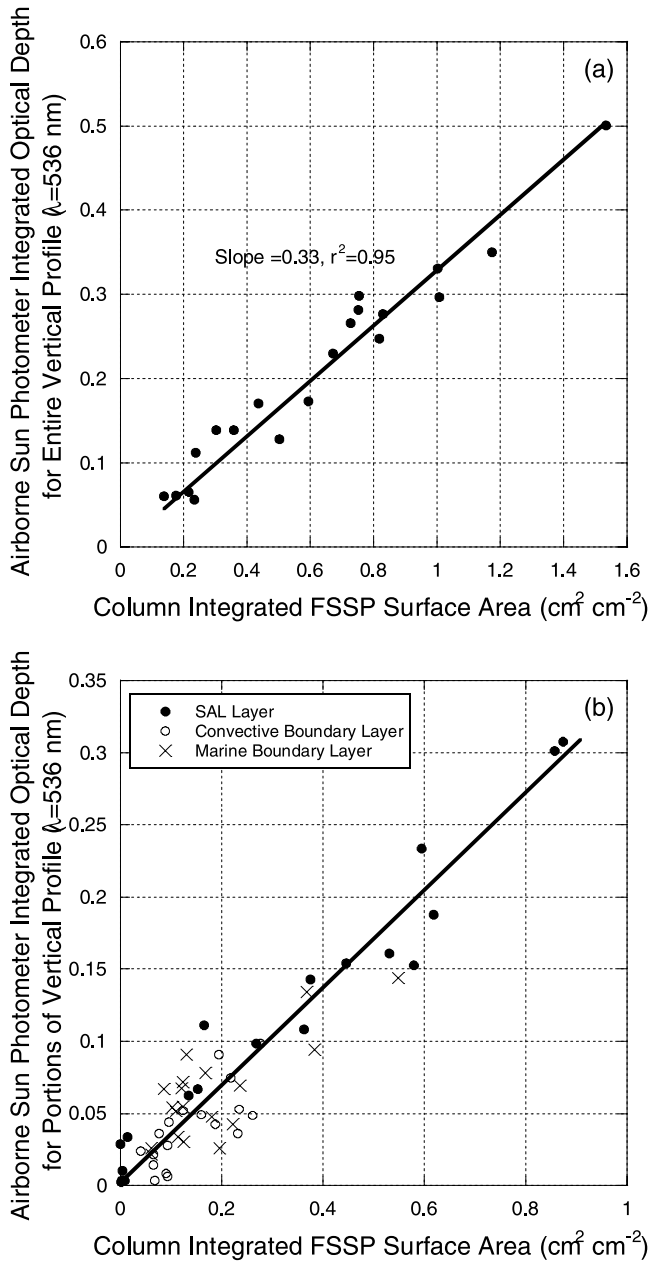

Figure 15. (a) Scatterplot of vertical profile aerosol optical thickness versus integrated particle surface area concentration. (b) Same as Figure 15a but for only portions of the vertical profile. These are broken up into the marine boundary layer (MBL), convective boundary layer (CBL), and Saharan Air Layer (SAL).

in Puerto Rico. Hence simply rebinning the FSSP will not decrease uncertainty in the results.

[76] It has also been suggested that OPCs yield diameters of equivalent cross sectional area for irregular particles. For example, *Pinnick and Rosen*, [1979] found in sensitivity studies in the laboratory using sphere doublets that for diameters larger than 4 μm the OPCs will size the particle relative to the equivalent cross-sectional area in the beam. This would certainly explain the very high correlation between the FSSP column integrated surface area and Sun photometer AOT. However, there are several of reasons why this cannot be applied to the FSSP. First, studies such as *Pinnick and Rosen* [1979] use a series of monodisperse sized particles with uniform index of refraction and hence a single response curve. Heterogeneous particles with varying index of refraction will add uncertainty. Despite the outstanding comparison between the FSSP and atmospheric extinction, there is one area of concern. The regression slope 0.33 cm^2 cm^{-2} in Figure 15 for AOT versus the particle surface area of the particles from the FSSP implies that dust has an extinction efficiency (Q_{ext}) of 1.3. If we account for particles smaller than the FSSP range, Q_{ext} becomes 1.1. This derived value of 1.1 is a factor of two too low when compared to the nominal value of 2 for coarse mode particles. Thus, on the basis of the ''diameter of equivalent cross-section'' model, the FSSP is still overestimating particle surface area by a factor of two, or equivalent surface area diameter by 40%.

[77] FSSP data shows that the equivalent area interpretation does not hold for OPCs, which measure size based on scattering from only a narrow field of view. The problem with the ''equal area'' hypothesis of *Pinnick and Rosen* [1979] when applied to the FSSP is that it is only valid for particle ranges where the fraction of light scattered into the detector angles is constant with size. Consider Figure 13b where the fraction of light scattered at detector angles is presented for the FSSP (4–12°) and some middle range instrument (say active scattering aerosol spectrometer probe ASASP at 35–120° used by *Pinnick and Rosen* [1979]). Here we see that for the ASASP, particles consistently scatter ~30% of their light at detector viewing angles for particles greater than ~3 μm in size. For the FSSP, this stability is not achieved until the 9 μm size is reached. Thus, if the true dust particle area distribution was not consistent during the PRIDE field study, the regressions in Figure 15 would probably not be as strong.

4.4. Inverted AERONET Sun/Sky Measurements

[78] Another goal of the PRIDE field campaign was to evaluate the *Dubovik and King* [2000] (hereafter referred to as DK) inversion under the difficult conditions of aspherical dust particles in a tropical location. During the PRIDE field campaign, the DK algorithm was able to successfully perform fifty-three inversions from the AERONET Sun photometer at Cabras Island which passed the automatic cloud screening algorithm. Only 17 passed the subsequent solar zenith angle restriction ($\zeta > 20°$) and the 21° sky radiance symmetry test. Solar zenith angles for the 17 valid inversions were grouped into two natural populations, those in the 27.9–29.0° range (10 occurrences), and those taken later in the day in the 60–75° range (7 occurrences). No more than 3 inversions were generated in any one particular day. The optical properties of inverted size distributions compared well with the measured sky radiances. Differences between computed and measured optical depths were 1.3 ± 0.1% and 2.0 ± 1.6% for the 28° and ~65° solar zenith cases, respectively. Differences between computed and measured radiance fields were 2.6 ± 0.7% and 4.1 ± 1.3% for the 28° and ~65° solar zenith cases, respectively.

[79] For comparison, the *Nakajima et al.* [1996] retrieval (hereafter referred to as N96) was also run for the same almucantar scans as the DK inversion. Of the 17 DK inversions used in this study, the N96 algorithm had only 10 solutions converge that passed the aureol symmetry tests (7 $\zeta = 28°$; 3 $\zeta = 65°$). Average errors for sky radiance were only slightly higher than DK, averaging 3.7 ± 1.4% and 3.7 ± 1.2%, for $\zeta = 28°$ and ~65°, respectively.

[80] Study average size distributions for turbid (AOT > 0.25), moderate (0.15 < AOT < 0.25) and clean marine (AOT < 0.15) are presented in Figure 16 for both the DK (Figure 16a) and N96 (Figure 16b) inversions. For average turbid conditions, the DK and N96 inversions give similar lognormal coarse mode size distributions with VMD = 4.0 and 3.9 μm and σ_g of 2.0 and 1.87, respectively. For moderate and marine conditions, inversions retained their shape (VMD = 4.2 and 3.8 μm, for DK and N96, respectively) and only reduced in amplitude.

[81] As the DK inversion was originally based on the N96 algorithm we expect on average the two to exhibit similar behavior. The most significant difference between the two inversions relates to the fine mode. Through the entire study the N96 retrievals show no sign of a fine mode whereas the DK inversion typically places an accumulation mode at 0.1 to 0.3 μm. On high AOT days, this fine mode from the DK inversions had an unrealistically small VMD < 0.20 μm (an artifact of the asymmetric nature of the particles [*Dubovik et al.*, 2002a]). On lower AOT days when dust was less prevalent, this mode also decreased in prominence and the VMD increased to a more reasonable value of 0.3 μm. Even when retrievals are restricted to low solar zenith angles, the dust asphericity effects in DK can still contaminate the fine mode. This fine mode artifact has been well documented by *Dubovik et al.* [2000], and we will not consider it further.

[82] While the mean size distributions appear stable and lognormal-like, the individual size inversions that made up the mean did show some variance. Examples of individual inverted size distributions for the DK and N96 inversions are presented in Figure 17. Figures 17a and 17b present all of the Cabras Island inversions for the ~28° and 65° degree solar zenith cases, respectively. When available, Figures 17c and 17d gives the corresponding N96 inversions.

[83] When dust was the dominant aerosol species in the atmosphere, (e.g., 9, 10, 15 July) both inversions produced single modal distributions with VMDs varying between 3.5 and 4.5 μm. Solar zenith angle in these cases did not appear to have a significant impact on either of the retrievals. However, on all other days when AOT < 0.25, we did find more variance. For example, for the $\zeta = 28°$cases, the DK solutions tended to thrash between 3 and 7 μm. In the some cases (such as 1 and 12 July), a more bimodal distribution becomes evident. The N96 inversion also showed variability in size for these cases although it retained much smoother shapes. For the higher zenith angles coarse mode solutions stabilized slightly. The DK solution smoothed considerably

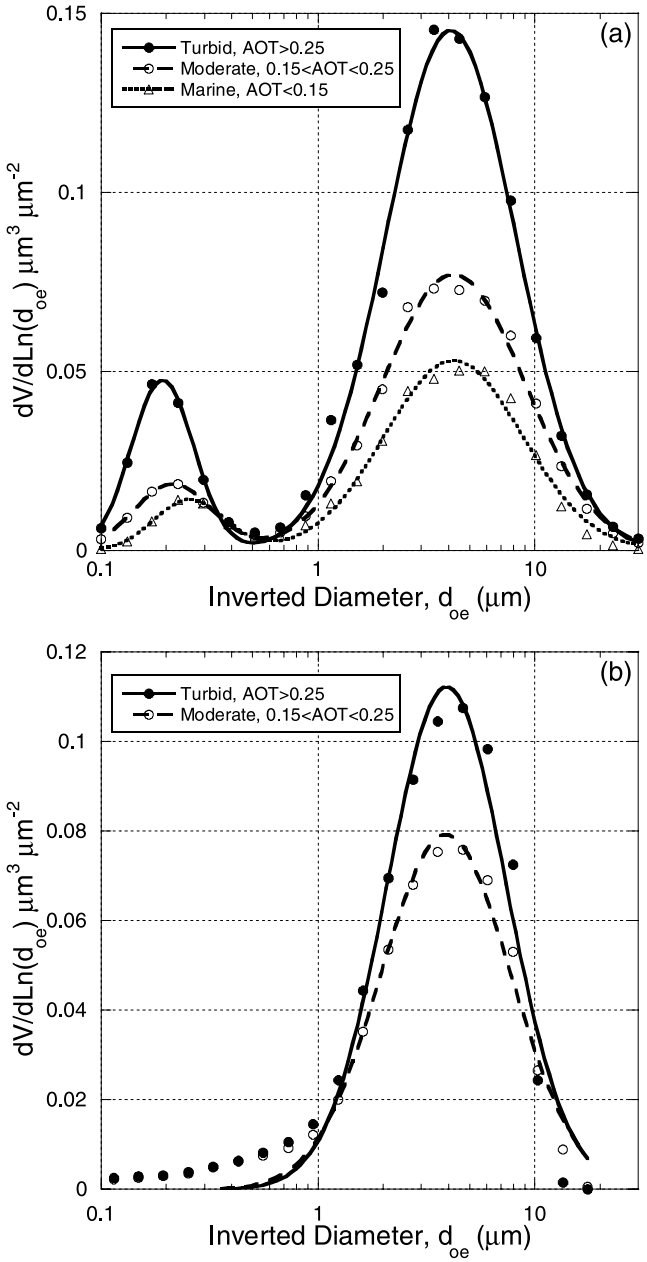

Figure 16. (a) Study averaged *Dubovik and King* [2000] and (b) *Nakajima et al.* [1996] study average inversions of dust particle size distributions at the Cabras Island site for high AOTs >0.25, moderate conditions with AOTs between 0.15 and 0.25, and clean marine airmasses with AOT < 0.15. There were no marine airmass cases for the Nakajima inversion. Curves from Figures 16a and 16b are not directly comparable as there are fewer Nakajima retrievals.

but still showed variability, with VMDs ranging from 3.5 to 6 μm. The N96 solution was remarkably stable, with VMDs at a static 3.8 μm.

[84] Because both the DK and N96 inversions specify some degree of smoothing in their inverted size distributions, it is initially unclear if the variability between some solutions is due to physical changes in the dust distribution or some artifact. Other instrumentation during PRIDE did not indicate any significant changes in dust size with time. In fact, there can be significant changes in retrievals only hours apart (such as 1 July in Figure 17b). Hence it is unlikely that these shifts are due to any natural variability in the dust. There are two potential artifacts, which might cause variability in these cases: cloud contamination, which escaped the clearing methods, and solution degeneracy. Cloud contamination can be a serious problem, particularly in the tropics where cirrus is prevalent. The *Smirnov et al.* [2000] screening algorithm principally used by AERONET has little difficulty screening optically thick clouds in the direct solar path by monitoring variability in the measured AOT over a two minute timescale. However, very thin (AOT < 0.03) and homogenous cirrus clouds can escape detection. For inversions, the situation is more complicated as the direct solar beam may be clear but cloud contamination can occur in the almucantar scan. The 21° symmetry test is a strong constraint to avoid these situations, however it is by no means perfect. If thin cirrus contamination did in fact occur, it would bias toward larger particles.

[85] Solution degeneracy is another potential problem. Inversions yield a best fit solution to the available sky radiance fields. However, it is possible that as dust is both an internal and external mix of aspherical particles, that several "homogeneous sphere" solutions may in fact give the same phase function. Clearly, in both the DK and N96 inversions, some compensation between optical parameters must occur.

[86] We can explore these issues by examining the phase functions of selected cases exhibiting the two "larger" and "smaller" particle states. Figures 18a and 18c present selected phase functions for the 28° and ~65° solar zenith angle inversions, respectively. Figures 18b and 18d are the corresponding ratios of these phase functions to those with the highest optical depth in their group (AOT = 0.4 and 0.3 for the 28° and 65°, respectively). For the 5° to 90° degree scattering regime, these phase functions exhibit similar characteristics regardless of their retrieved size distribution shape or solar zenith angle of the retrieval. Individual curves vary by less than 10% from one another. Strong divergence appears in two areas: scattering angles <5°, and scattering angles > ~110°. At the larger scattering angles, there is a considerable amount of variance from retrieval to retrieval-spanning as much as a factor of two in some cases. These differences are not a function of solar zenith angle, nor are they related to the two size states. Consider that qualitatively the 30 June and 9 July inversions in Figure 18a look very similar in shape and size. The resulting phase functions are strongly different for scattering angles greater than 130°. As sky radiance is not measured for scattering angles larger than ~125°, these perturbations are simply extrapolations based on Mie theory from the inverted size distribution. This demonstrates how sensitive the phase function at larger angles can be to small changes in retrieved size and index of refraction.

[87] These findings suggest perturbations for the low scattering angles as the likely causal factor. As expected, the amplitude of the phase functions appears to be strongly related to the median size of the volume distributions. For example, the distributions with the largest particle sizes (8 and 14 July in Figure 17a and 11 July in Figure 17b) also had the largest volume median diameters. However, here too phase functions in the far forward are an extrapolation-

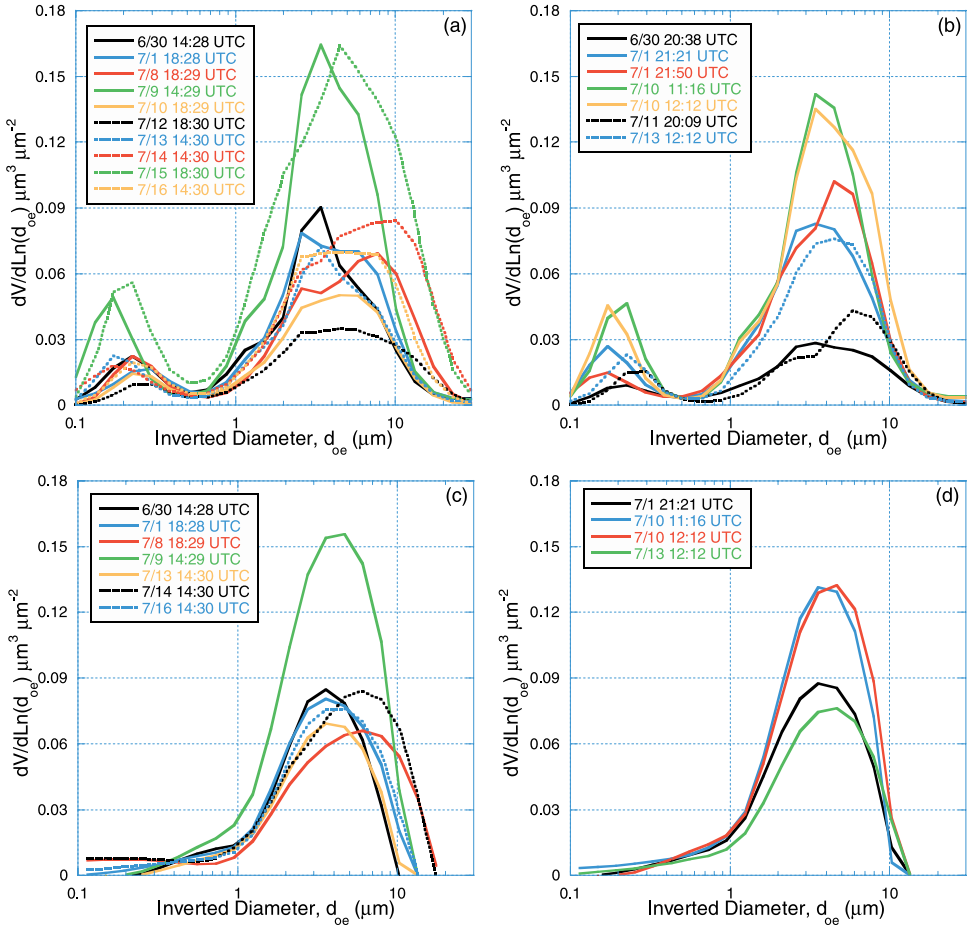

Figure 17. Sample inverted size distributions from AERONET Sun/sky measurements at the Cabras Island site using the *Dubovik and King* [2000] and *Nakajima et al.* [1996] inversions. (a) *Dubovik and King* [2000] inversions using only data with solar zenith angle (ζ) near 28° range. (b) *Dubovik and King* [2000] inversions using only data with solar zenith angle near the 65°. (c) Same as Figure 17a for available *Nakajima et al.* [1996] inversions. (d) Same as Figure 17b for available *Nakajima et al.* [1996] inversions.

almucantar data is only used for scattering angles >5°. Hence the small perturbations in the ~5–120° range are driving the inversion variations.

[88] Finally, we cannot escape the issue that these are aspherical particles and that if this is taken into account, the solutions will improve. Recently, *Kalashnikova and Sokolik* [2002] found that dust particles likely have increased scattering in far forward angles relative to spheres-on the order of 15–50%. As the DK and N96 codes assume homogenous spheres, it is possible that these variations in the size distribution depend on the weight these small scattering angles have on the fit. To test this final hypothesis, the latest version of the DK code was run which accounts for some asphericity effects by assuming spheroidal particles with an average aspect ratio of 1.9 (this modification is described by *Dubovik et al.* [2002b]). Figure 19 presents volume distributions for the seven cases shown in Figure 17b (this retrieval is only run for $\zeta > 40°$). Aside from the diminishing of the accumulation mode artifacts, the distribution shapes look fairly similar. The largest difference is evident in the two 1 July cases, where instead of having a "large" and "small" diameter distribution in the spherical model, a more bimodal shape is derived in the spheroidal model.

[89] After this analysis it is still unclear which size distribution is "correct". All that can be said is that these inversions reproduce the sky radiance data for scattering angles of ~5–120°. Shifts and differences in the particle size retrievals raise questions as to what it is the inversions are retrieving and how it should be used. Certainly one must consider that it is a column integrated size distribution and includes undetected cirrus, sea salt in the MBL which changes size as a function of relative humidity and hence altitude, and dust which also likely changes in size with altitude through some gravitational mechanism. However, even this is a simplification of the problem. The sky retrieval is done on the radiance from the whole atmospheric column and the best fit is done taking into account all available information. At the writing of this paper, it is unclear whether we are biasing our analysis if we only utilize the single modal solutions and subjectively dismiss the bimodal solutions as "cirrus contaminated." We must accept these variations as fundamental uncertainties in the method. Taken over a study average, they do not significantly alter

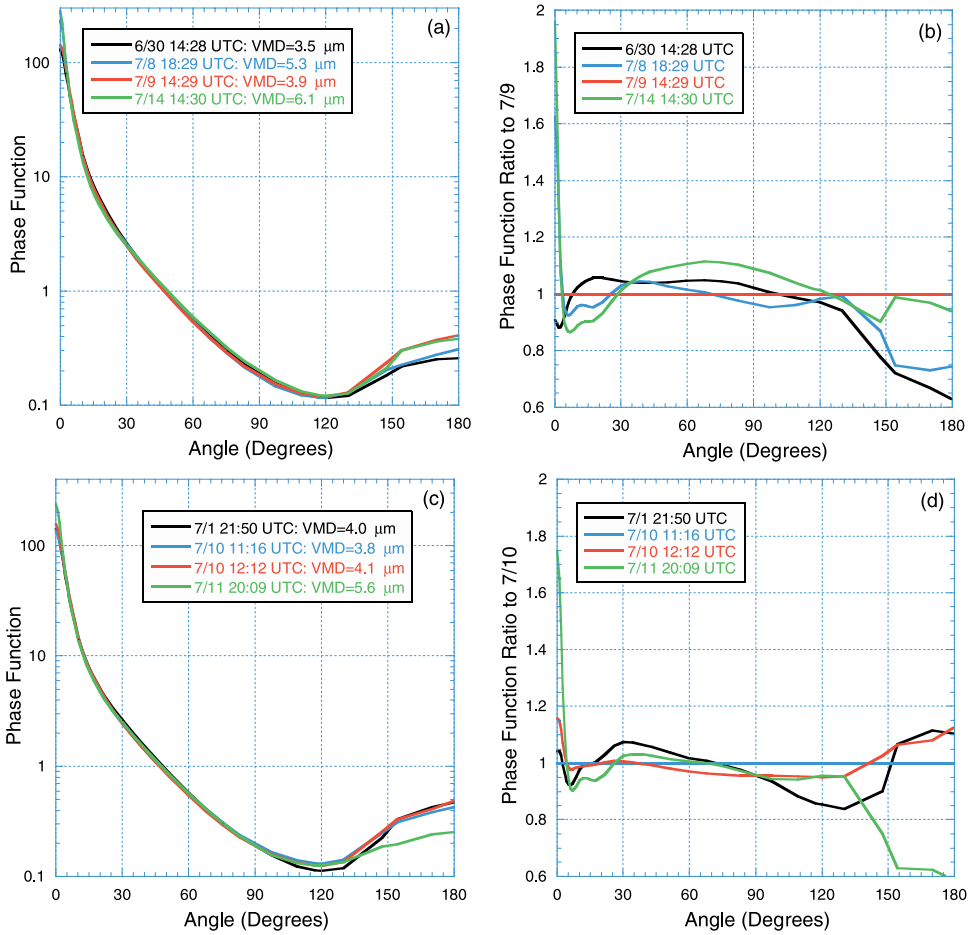

Figure 18. (a) Phase functions derived from *Dubovik and King* [2001] inversions for zenith angles of ~28°. (b) Phase functions from Figure 18a normalized to the 9 July case. (c and d) The same as Figures 18a and 18b but for solar zenith angles >59° and normalization to the 10 July case.

the mean distribution, although clearly care must be taken on treating individual inversions. However, if inversions are understood to be an optical equivalent distribution, these issues may not be important if the data is applied in the proper context.

5. Discussion on the Differences in Measured Size Distributions

[90] In the previous section we have discussed in detail the measured size distributions from the most commonly used techniques. In some cases, dust particles clearly present unrecoverable artifacts. In others, issues on the context data should be taken also makes dust particle "size" an ambiguous term. Consider Figure 20 where we have displayed mean volume distributions from the various methods described in this study. Here we normalized all of the volume distributions to unity and made corrections to geometric diameter from the aerodynamic methods by using the factor of 1.4 we have employed previously. By comparing these methods in this way, the true variance becomes clear. Particle modes vary from 2 to 10 μm and everywhere in between. Shape functions also vary to a large extent from smooth curves for the inversions to the more jagged distributions from the DRUM and FSSP.

[91] As can be seen from Figure 20 and the discussions in section 4, there are tremendous differences in measured size distributions, and it is unclear which, if any, should be used. Further, if a size distribution is "incorrect" is the data still valuable or totally without merit? In the previous sections we have answered these questions in part. Certainly, the FSSP data is an outlier and must be used with caution. Similarly, geometric sizing probably over sizes and can probably be dismissed for use in this context and as we discussed, the DRUM sampler probably under sizes due to particle breakup and inlet issues. This leaves the MOUDI impactor, the APS and the Sun-sky inversions. However, even these are probably biased. The MOUDI most likely had inlet issues, which suggests that it is biased toward smaller particles. The APS may also be in error, but because the factor of "1.4" between aerodynamic and geometric is a best fit from previous data, and the bias has been empirically corrected for, many sizing questions are left unanswered. Because inversions are based on spherical or spheroidal geometries, it is unclear whether they are biased toward larger or smaller particles (recall, that this distribution is the "mean" between two states).

[92] Based on all of these observations, we could average and weigh these distributions and determine a "best fit" solution. Subjectively, we would place a volume median/

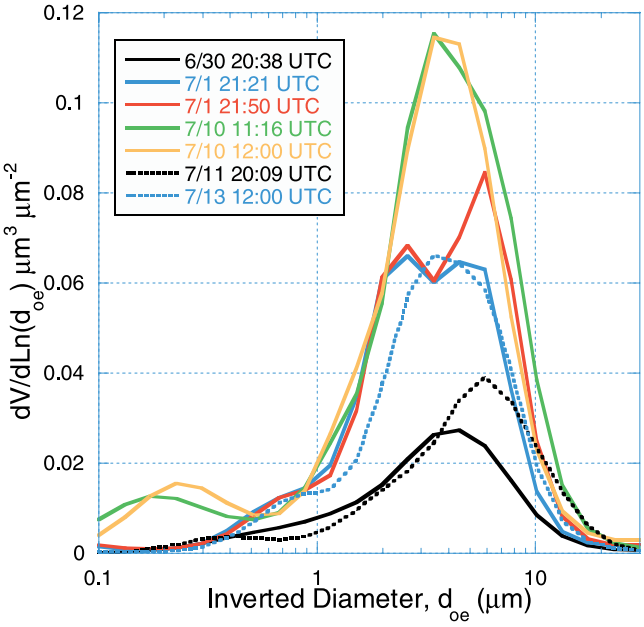

Figure 19. *Dubovik and King* [2000] method inversions for PRIDE where spheroidal particles are assumed instead of spheres using the *Dubovik et al.* [2002b] correction. These inversions are only recommended for solar zenith angles in excess of 40°.

mass median diameter over Puerto Rico at ~3.5 ± 0.6 μm, and a geometric standard deviation of ~2.1. However, does such an approximation make physical sense? Certainly by evaluating the electron microscopy data such a value is physically small (regardless of morphology issues). What is then the meaning of a "volume distribution?"

[93] Given the size distributions in Figure 20, and the sensitivity of the mass extinction efficiency to size in Figure 1 (e.g., linear in the mass median/volume median diameter), it is clear that modelers are left with a problem; even a small error in the modeled size distribution, say from 3 to 4 μm, will lead to a 33% error in computed optical depths. The implications are clear: in a model/AERONET/satellite intercomparison, are the differences between the model and validation data due to errors in the scattering, or in the original dust mass flux? These difficulties leads us to invert the problem: Given that we know the size distribution is uncertain, let us consider the measured values of the particle mass extinction efficiency and use it as a constraint.

[94] *Maring et al.* [2000] measured the Saharan dust mass scattering efficiency at 550 nm to be 0.5 ± 0.1 m^2 g^{-1} in Tenerife, Canary Islands. *Li et al.* [1996] found 0.6 ± 0.1 m^2 g^{-1} during a very heavy dust event several thousand kilometers away in Barbados. Given a mass absorption efficiency of ~0.08 m^2 g^{-1} (Savoie et al., submitted manuscript, 2003) this implies an average mass extinction efficiency in the 0.6–0.7 m^2 g^{-1}range. In Puerto Rico during PRIDE, Savoie et al. (submitted manuscript, 2003) found that after transporting across the Atlantic some large particles were scavenged and the average mass extinction efficiency increased to −0.7–0.8 m^2 g^{-1}. Now, consider again Figure 1a, which assumes spherical geometry. Assuming an estimated density for dust minerals on the order of ~2.7 g cm^{-3}, this would imply that on the coast of Africa, dust would have a volume mean diameter on the order of ~2.75 μm. If we use the PRIDE values as a constraint, this value drops even lower, to ~2.25 μm. This is considerably lower than our rough estimate based on the particle sizing probes of 3.5 μm, which would have a mass extinction efficiency 0.5 m^2 g^{-1}, or the electron microscopy data which would suggest <0.3 m^2 g^{-1}. Hence none of the methods are reproducing the correct mass extinction efficiency. Thus any subsequent modeling of dust optical depth in transport models will be in error by the same amount.

[95] This discrepancy is troubling. On the basis of all of the size data (including the electron microscope), the mass/volume median diameter cannot be as low as 2.25 μm. Dust particles are likely several microns larger. This implies then that perhaps the mass extinction efficiency is in error. However, we find that these are reasonable values for airborne dust. As a particle becomes more asymmetrical, its surface area to volume ratio increases thus implying more scattering per unit mass. Spheroidal modeling studies based on equivalent surface area and volume sizes suggested that particle asphericity would not effect the computation of the bulk scattering or absorption coefficient [e.g., *Mischenko et al.*, 1997; *Pilinis and Li*, 1998]. However, there is evidence that this is not true. Most recently, theoretical studies by *Kalashnikova and Sokolik* [2002] have suggested that by using irregularly shaped particles, k_{ext} for individual particles can be as much as 30% higher than similarly computed spheroids. There is mounting experimental evidence to support this claim. *Maring et al.* [2000] found that spherical Mie calculations based on an APS data in Tenerife systematically underestimated light scattering by 20%. Considering that they correct their nephelometer for truncation errors assuming a spherical geometry, and that particle nonsphericity greatly heightens the phase function for angle less than 10°, this discrepancy is probably on the order of 25% (in better agreement with theory).

[96] We can correct these issues, such as the mass extinction efficiency or even the phase functions for indi-

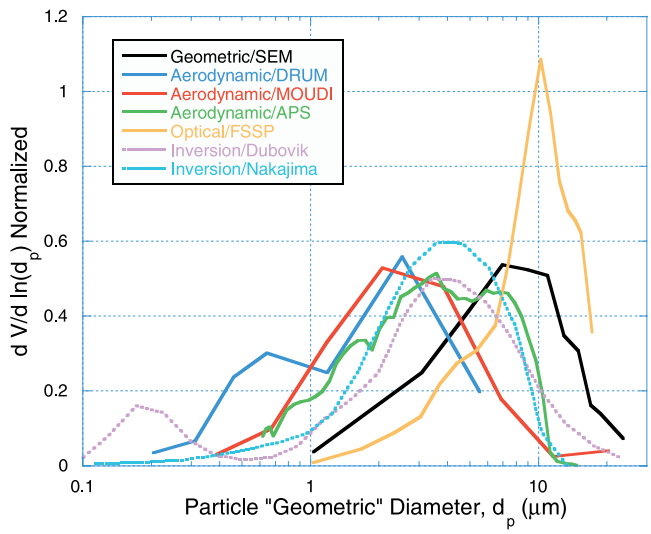

Figure 20. Intercomparison of average dust volume distributions from all of the methods discussed in this study.

vidual size distributions, by simply making an empirical perturbation to scattering calculations by again applying some effective density correction (perhaps use 2 g cm^{-3} instead of 2.7 g cm^{-3}, as we do for the aerodynamic conversion). However, if this must be done for each data set and instrument, then the ''corrected'' size distribution or scattering/absorption calculations becomes somewhat subjective. We are still left with the fundamental questions such as what is the meaning of dust size distribution measurements and how should they be applied. In most atmospheric climate models airborne particles are modeled as a size distribution (or distribution parameter) and an estimated index of refraction. Let us consider each of the methods individually.

5.1. Single Particle Analysis

[97] Single particle analysis offers a powerful tool for analyzing the properties of dust particles. However, there is a great deal of subjectivity in interpreting the data. Of all of the methods, sizing by single particle analysis is the most ambiguous. This is compounded by the plate-like nature of clay minerals. If one uses a ''diameter of equivalent cross sectional area'' particles will no doubt be biased high. Since images are two dimensional, equivalent volume diameters are difficult to construct. Impact/shatter issues also make the derivation of particle morphology in its natural state uncertain. Most importantly, single particle analysis cannot be used to derive a particle concentration, only a normalized distribution can be generated (filter inhomogeneity effects make the derivation of a concentration very uncertain for these types of particles).

5.2. Optical Particle Counters

[98] Optical particle counter data most likely has the largest biases and most likely is the most difficult to correct for size. Despite the large quantity of airborne data using these instruments (it is difficult to make aerodynamic measurements on airborne platforms), most of it probably cannot be applied to radiative transfer calculations. The very large discrepancy in particle size and hence optical properties like mass extinction efficiency or even single scattering albedo (e.g., Figure 1b) makes ''column closure'' for dust in the classical sense almost impossible. OPCs have their place in research in their capacity as single particle counters and a wealth of qualitative data can be derived. Further, OPCs do generate a quantifiable pulse height distribution and some optical and some size information can be derived.

[99] Based on the discussion in section 4.3, it appears that FSSP data in particular on dust particles must be used with extreme caution. Not only does this suggest a reevaluation of previous studies that employed this particular instrument to measure dust, but also, based on the findings of Table 1, perhaps all OPC studies should be reexamined. For example, *Ackerman and Cox* [1982] used a FSSP to measure dust properties in the Persian Gulf region. Their size distribution was nearly identical to those presented here. However, these findings do not necessarily imply that all OPC data in the literature is in error, but rather should be reevaluated on a case by case basis. Each instrument has its own characteristics. Instruments that use white light instead of a coherent laser beam would probably not have as much difficulty with the Mie peaks. Wider viewing angles are also preferable. However, in these cases index of refraction corrections may not be straightforward.

5.3. Inverted Size Distributions

[100] The inverted AERONET size distributions from the *Dubovik and King* [2000] and *Nakajima et al.* [1996] gave mean size distributions in the middle of those measured in PRIDE. During the PRIDE campaign they matched sky radiance values well and in the case of the N96 inversion even optical depth was within 5%. (DK is constrained to optical depth). Further, given that the impactors probably underestimated size, these may very well be closer to the ''true'' size distribution. However, interpreting and applying these results is not straightforward.

[101] While in situ instruments like OPCs and filter samples can give particle number and mass concentrations which are tangible, column integrated inversions do not give a solution which can be easily linked to particle microphysics. These are best fit solutions, and any changes in particle size have consequences in the column-integrated volume. For example, the calculated mass extinction efficiency for the four highest AOT inversions assuming a density of 2.7, (say for optical depths above 0.25), gives a mean value of 0.51, 0.44, and 0.53 m^2 g^{-1} for the N96, DK spherical and DK spheroid, respectively, or about 33% low.

[102] This leaves us with a predicament: Inversions are constrained by the radiation field. If we apply an effective density of say, 2 g cm^{-3} to adjust to the correct mass extinction efficiency, we are still left with the incorrect particle number, area and volume in the atmosphere. Or, if we change the volume, we no longer have a closure with optical depth. Regardless there is no simple method to keep inverted size distributions consistent with the microphysics. For lower optical depth situations when sea-salt becomes a more significant species, or if there is a mix between fine mode particles and dust the situation becomes considerably more complicated.

[103] As transport models do not use optical depth as an independent variable, use of the current generation of inversion solutions as initial size distributions in such models is problematic. As inversion solutions compare well with AOT and sky radiance it is fair to say that it can be employed in radiative transfer calculations for sky radiance and downward flux at the surface. As to how physical the solution is and if it can be applied to other radiative problems such as radiative transfer involving satellite remote sensing is also complicated. As was shown in Figure 18, small changes in retrieved size distributions may not affect derived phase functions for scattering angles less than 100° as these are incorporated in the retrieval. However, extrapolations using these size distributions at larger angles can cause variances by ~20 or 30%. Compound this with dust asphericity issues which makes such extrapolations very uncertain.

[104] Despite these shortcomings and uncertainties in the retrievals we must recognize the size, consistency and geographic extent of Sun/sky retrievals such as the AERONET database. Because of a general lack of consistent aerosol data globally, the inverted dust size distributions have their place in research. Indeed, *Tanre et al.* [2001], *Dubovik et al.* [2002a], and *Smirnov et al.* [2002] have published thorough climatologies of dust properties using these

inversion methods. The strength of this method is that all things being equal, size distributions from differing regions of the world can be compared and inferences be made as to relatively how particles are changing in size and microphysics from place to place. However, the findings of this study show that these distributions cannot simply be placed into a transport or similar global climate model to determine dust direct forcing without incurring significant uncertainties.

5.4. Aerodynamic Methods

[105] Despite the sizing and inlet issues with impactors during PRIDE, aerodynamic methods are probably the most useful for describing the properties of dust. While, these methods have been used for decades, recent developments and proliferation of single particle counters and inversions has caused these fundamental measurements to decline in prevalence. Of all of the "equivalent diameter" parameterizations, aerodynamic diameter is the most well defined. There are few calibration issues; it simply is an inherent property of the particle. Similarly, mass concentration is a quantifiable entity. If done properly, mass concentration measurements probably have the lowest uncertainty. There are no issues of shape factors, only signal-to-noise issues. It is partly for this reason that regional air quality monitoring has emphasized this parameterization method for many decades. Perhaps for complicated dust particles a "back to basics" microphysics approach is needed.

[106] Consider the current needs of the scientific community. The problem most often discussed is that dust direct forcing estimates have one of the largest uncertainties of any aerosol species [*IPCC*, 2001]. Can we determine dust direct forcing not only globally, but also at an individual point? To this end, global climate and mesoscale models have been run with various source functions, size distributions and chemistries. Similarly, those in the remote sensing communities require knowledge of dust scattering and absorption properties. Ultimately, these two methods will need to be combined. Optical depth measurements from satellites will be used in conjunction with transport models for validation and eventually to derive dust fluxes. Mass estimations from models need to be compared to satellite short-wave flux measurements to determine radiative forcing. The most important dependent parameters to unify the modeling and remote sensing techniques are most likely the mass scattering and mass absorption efficiencies, followed by the scattering phase function. Using mass as a function of aerodynamic diameter as the primary independent variable to relate to these parameters is not only the most direct and efficient method, but probably best utilizes the community data set. For example, one must consider that dust-wind speed flux parameterizations used in transport models have mostly been based on fundamental mass measurements. These are most commonly filter and cascade impactor measurements, which measure mass as a function of aerodynamic size to begin with.

[107] Most climate and mesoscale models parameterize particles simply with a spherical particle model number concentration with diameter, density, and index of refraction. This allows for direct calculation of radiative properties. However, particle dry and wet scavenging as well as other aerosol modifying mechanisms are functions of aerodynamic diameter. Models then convert from geometric to aerodynamic diameter for these calculations. It may be more direct to simply utilize mass instead of number, and aerodynamic diameter instead of geometric diameter, and then convert to optical diameter for radiative calculations. Mathematically, these two points of view can be viewed as equivalent when one evokes a spherical model. However, dust particles are decidedly nonspherical, and are not described well by Mie Theory. Hence models must focus on either mass or number as an independent variable, and by utilizing one will cause more uncertainty in the other.

[108] Admittedly, the transfer function between aerodynamic and optical equivalent diameter such that the models can be unified with remote sensing can be difficult. However, the other sizing methods described in this study probably cannot easily produce an optical equivalent size distribution that would be useful for remote sensing either. The only consistent result of theoretical studies of dust particle scattering phase functions is simply that dust particles scatter differently from spheres. There are clear tendencies, such as the additional amount of scattering in the <10 and $90-140$ -degree range followed by a decrease for scattering angles $>140^\circ$ [e.g., *Mishchenko et al.*, 1997; *Kalashnikova and Sokolik*, 2002]. However, the question is whether such refinement can find its way into models into any meaningful way. If so, such a transfer function between particle number, mass, and scattering would no doubt be complicated and to some degree subjective. Establishing an empirical relationship between mass scattering, mass absorption and phase function as a function of aerodynamic diameter may be the most direct and reliable method currently available.

[109] Number counting aerodynamic sizers such as the APS certainly have a place in research as well. Their high time and size resolution certainly makes them useful. For the PRIDE study, the APS was one of the most reliable instruments deployed and can no doubt detect even small changes in a particle size distribution. However, like the optical particle counters as an "individual particle counter" there can be ambiguity in interpreting results. For example, was a particular particle event from dust or sea salt? Is the bimodal behavior real or due to differing particle reactions to the accelerating flow in the instrument? These issues can be circumvented if the APS is applied consistently. For example, *Maring et al.* [2003a] compared APS size distributions at Tenerife, Canary Islands, to the data collected at Puerto Rico during PRIDE. From these he could accurately estimate changes to the particle size distribution during transport.

[110] These arguments on the use of mass as a function of aerodynamic diameter may appear straight forward, but we concede that in practice there can be difficulties. Indeed, in this very study we showed the impactors to suffer from inlet issues, bounce-off, and other biases. This resulted in only 60% of the dust particle mass being retrieved, making them some of the less reliable data from the PRIDE study. These methods also suffer from being time and labor intensive, and are not easily implemented in airborne systems, (which is where dust size data are most needed). In the historical data set we are often without the benefit of auxiliary data for us to determine if the presented data is biased (probably most of the aerodynamic data in Table 1 is accurate).

However, these are all issues that are well defined and treatable, whereas other methods, such as OPCs and optical inversions, have poorly defined problems and may be untreatable.

6. Summary and Conclusions

[111] In this study we compare dust size distributions from geometric, aerodynamic, and optical methods. Large differences were found, particularly between optical particle counters and the aerodynamic methods. A review of other size distributions in the literature shows that this is a consistent bias in the community data sets. A summary of individual system performance and implications is as follows.

[112] 1. Geometric sizing of particles by electron microscopy techniques likely biases particles toward larger sizes. Size parameters have a high degree of ambiguity.

[113] 2. Both the MOUDI and DRUM cascade impactors most likely suffered from inlet/system losses on the order of 40%. The DRUM sampler most likely also suffered from particle breakup on impact, resulting in daughter particles being collected at smaller sizes.

[114] 3. The aerodynamic particle sizer (APS3300) proved to be one of the most reliable sizing methods for the study. However, ambiguities arise from its inability to separate out dust from sea salt on individual samples.

[115] 4. The airborne FSSP-100 consistently oversized dust particles by more than a factor of two. This is due to a combination of effects including low response for particles in the 3–10 μm range, and index of refraction and shape ambiguity on a particle by particle basis. While this bias excludes its use for radiative transfer calculations, it is nevertheless a useful tool in determining dust number concentration, vertical profile and light scattering. A review of the literature shows that this error is not only confined to the FSSP, but potentially to other coarse mode optical particle counter systems as well.

[116] 5. Inversions from AERONET Sun/sky data using the *Nakajima et al.* [1996], *Dubovik and King* [2000], and the Dubovik and King spheroid retrievals give consistent mean size distributions in the middle of the methods tested. However, there was variability on a retrieval by retrieval basis. At this time it is unclear whether this is due to nonvisible cirrus contamination or due to potential degeneracy in the retrieved solution (i.e., two different solutions describe the Sun/sky environment nearly identically).

[117] 6. None of the methods compared in this study can adequately reproduce the measured mass extinction or mass scattering efficiency of the dust using spherical geometry methods. Utilizing such methods lead to ~30% underestimate of particle scattering. This is contrary to what is commonly assumed. Our results are consistent with recent theoretical and experimental work.

[118] 7. Given all of the uncertainties in the sizing methods, we promote the use of fundamental and quantifiable descriptors of particles. In particular, the use of mass as a function of aerodynamic diameter seems to be the most well definable relationship. Bulk mass scattering and absorption efficiencies plus precalculated phase functions can then be utilized to describe the radiative environment.

[119] 8. Finally, we may have to accept the inherent uncertainties of the dust measurements. Given the staggering number of free variables in the physical parameters of dust (size, shape, chemistry, vertical distribution) it is clear that no forward model on its own can completely capture the complicated nature of dust's radiative effects. Indeed, as clearly shown by *Tegen et al*. [1996] and *Myhre and Stordal* [2001] there is very little room for error in assumed physical parameters and particle microphysics. However, these are indications that we as a community need to make special efforts in making these critical measurements.

[120] **Acknowledgments.** We are grateful to all of the personnel who participated in the PRIDE field campaign. Special thanks are due to Aaron Broumas at the University of California for the SEM samples for this study, Kevin Perry at the University of Utah for helping with the analysis of the DRUM data, and Migel Izaguirre and Lillian Custals of the University of Miami for their maintenance of the Cabras Island surface site. We appreciate the comments of Dean Hegg, of the University of Washington and Richard Paulus, SSC-SD. PRIDE funding was provided by the Office of Naval Research, Code 322, N0001401WX20194.

References

Ackerman, S. A., and S. K. Cox, The Saudi Arabian Heat Low: Aerosol distribution and thermodynamic structure, *J. Geophys. Res.*, *87*, 8991–9002, 1982.

Anderson, J. R., P. B. Buseck, T. L. Patterson, and R. Arimoto, Characterization of the Bermuda tropospheric aerosol by combined individual-particle and bulk aerosol analysis, *Atmos. Environ*, *30*, 319–338, 1996.

Arimoto, R., B. J. Ray, N. F. Lewis, U. Tomza, and R. A. Duce, Mass-particle size distributions of atmospheric dust to the remote ocean, *J. Geophys. Res.*, *102*, 15,867–15,874, 1997.

Baron, P. A., Calibration and use of the aerodynamic particle sizer (APS 3300), *Aerosol Sci. Technol.*, *5*, 55–67, 1986.

Baron, P. A., M. K. Mazumder, and Y. S. Cheng, Direct reading techniques using optical detection, in *Aerosol Measurement: Principles, Techniques, and Applications*, edited by K. Willeke and P. A. Baron, pp. 381–409, Van Nostrand Reinhold, New York, 1993.

Brock, C. A., J. C. Wilson, and W. R. Seebaugh, Measurements of aerosols and clouds from aircraft, in *Aerosol Measurement: Principles, Techniques, and Applications*, edited by K. Willeke and P. A. Baron, pp. 690–704, Van Nostrand Reinhold, New York, 1993.

Brockman, J. E., Sampling and transport of aerosols, in *Aerosol Measurement: Principles, Techniques, and Applications*, edited by K. Willeke and P. A. Baron, pp. 77–111, Van Nostrand Reinhold, New York, 1993.

Cahill, T. A., C. Goodart, J. W. Nelson, R. A. Eldred, J. S. Nasstrom, and P. J. Feeny, Design and evaluation of the DRUM impactor, in *Proceedings of the International Symposium on Particulate and Multi-Phase Processes*, vol. 2, edited by T. Ariman and T. Nejat, pp. 319–325, Taylor and Francis, Philadelphia, Pa., 1985.

Cahill, T. A., T. E. Gill, D. A. Gillette, E. A. Reid, J. S. Reid, and M. L. Yau, Generation, characterization and transport of Owens (dry) Lake, final report, *Contract A132-105*, Calif. Air Resourc. Board, Sacramento, Sept. 1994.

Carlson, T. N., and R. S. Caverly, Radiative characteristics of Saharan dust at solar wavelengths, *J. Geophys. Res.*, *82*, 3141–3152, 1977.

Claquin, T., M. Schulz, Y. Balkanski, and O. Boucher, Uncertainties in assessing radiative forcing by mineral dust, *Tellus, Ser. B*, *50*, 491–505, 1998.

Colarco, P., et al., Saharan dust transport to the Caribbean during PRIDE: 2. Transport, vertical profiles, and deposition in simulations of in situ and remote sensing observations, *J. Geophys. Res.*, *108*, doi:10.1029/2002JD002659, in press, 2003.

Collins, D. R., et al., In situ aerosol-size distributions and clear-column radiative closure during ACE-2, *Tellus, Ser. B.*, *52*, 498–525, 2000.

Coude-Gaussen, G., P. Rognon, G. Bergametti, L. Gomes, B. Strauss, J. M. Gros, and G. M. Le-Coustumer, Saharan dust on Fuerteventura Island (Canaries): Chemical and mineralogical characteristics, air mass trajectories, and probable sources, *J. Geophys. Res.*, *92*, 9753–9771, 1987.

D'Almeida, G. A., On the variability of desert aerosol radiative characteristics, *J. Geophys. Res.*, *92*, 3017–3026, 1987.

D'Almeida, G. A., and L. Schutz, Number, mass and volume distributions of mineral aerosols and soils of the Sahara, *J. Clim. Appl. Meteorol.*, *22*, 233–243, 1983.

Davies, C. N., Particle fluid interaction, *J. Aerosol Sci.*, *10*, 477–513, 1979.

Dubovik, O., and M. D. King, A flexible inversion algorithm for retrieval of aerosol optical properties from Sun and sky radiance measurements, *J. Geophys. Res.*, *105*, 20,673–20,696, 2000.

Dubovik, O., A. Smirnov, B. N. Holben, M. D. King, Y. J. Kaufman, T. F. Eck, and I. Slutsker, Accuracy assessment of aerosol optical properties retrieval from AERONET Sun and sky radiance measurements, *J. Geophys. Res.*, *105*, 9791–9806, 2000.

Dubovik, O., B. N. Holben, T. F. Eck, A. Smirnov, Y. J. Kaufman, M. D. King, D. Tanre, and I. Slutsker, Variability of absorption and optical properties of key aerosol types observed in worldwide locations, *J. Atmos. Sci*, *59*, 590–608, 2002a.

Dubovik, O., B. N. Holben, T. Lapyonok, A. Sinyuk, M. I. Mishchenko, P. Yang, and I. Slutsker, Non-spherical aerosol retrieval method employing light scattering by spheroids, *Geophys. Res. Lett.*, *29*(10), 1415, doi:10.1029/2001GL014506, 2002b.

Falkovich, A. H., E. Ganor, Z. Levin, P. Formenti, and Y. Rudich, Chemical and mineralogical analysis of individual mineral dust particles, *J. Geophys. Res.*, *106*, 18,029–18,036, 2001.

Fouquart, Y., B. Bonnel, M. Chaoui Roqual, R. Santer, and A. Cerf, Observations of Saharan aerosols: Results of ECLATS field experiment. part I: Optical thickness and aerosol size distribution, *J. Clim. Appl. Meteorol.*, *26*, 28–37, 1987.

Ganor, E., H. A. Foner, S. Brenner, E. Neeman, and N. Lavi, The chemical composition of aerosols settling in Israel following dust storms, *Atmos. Environ.*, *25*, 2665–2670, 1991.

Gao, Y., and J. R. Anderson, Characteristics of Chinese aerosols determined by individual-particle analysis, *J. Geophys. Res.*, *106*, 18,037–18,045, 2001.

Ginoux, P., M. Chin, I. Tegen, J. M. Prospero, B. Holben, O. Dubovik, and S. J. Lin, Sources and distributions of dust aerosol simulated with the GOCART model, *J. Geophys. Res.*, *106*, 20,255–20,273, 2001.

Gomes, L., and D. A. Gillette, A comparison of characteristics of aerosol from dust storms in central Asia with soil derived dust from other regions, *Atmos. Environ., Part A*, *27*, 2539–2544, 1993.

Gomes, L., G. Bergametti, G. Coude-Gaussen, and P. Rognon, Sub-micron desert dusts: A sandblasting process, *J. Geophys. Res.*, *95*, 13,927–13,935, 1990.

Gullu, G. H., I. Olmez, and G. Tuncel, Chemical concentrations and elements size distributions of aerosols in the eastern Mediterranean during strong dust storms, in *The Impacts of Desert Dust Across the Mediterranean*, edited by S. Guerzoni and R. Chester, pp. 339–347, Kluwer Acad., Norwell, Mass., 1996.

Hinds, W. C., *Aerosol Technology, Properties, Behavior and Measurement of Airborne Particles*, pp. 38–68, John Wiley, New York, 1982.

Holben, B. N., et al., AERONET—A federated instrument network and data archive for aerosol characterization, *Remote Sens. Environ.*, *66*, 1–16, 1998.

Holben, B. N., et al., An emerging ground-based aerosol climatology: Aerosol optical depth from AERONET, *J. Geophys. Res.*, *106*, 12,067–12,097, 2001.

Intergovernmental Panel on Climate Change (IPCC), *Climate Change 2001: The Scientific Basis*, edited by J. T. Houghton et al., Cambridge Univ. Press, New York, 2001.

Kalashnikova, O. V., and I. N. Sokolik, Importance of shapes and compositions of wind-blown dust particles for remote sensing at solar wavelengths, *Geophys. Res. Lett.*, *29*(10), 1398, doi:10.1029/2002GL014947, 2002.

Kaufman, Y. J., A. Gitelson, A. Karnieli, E. Ganor, R. S. Fraser, T. Nakajima, S. Mattoo, and B. N. Holben, Size distribution and scattering phase function of aerosol particles retrieved from sky brightness measurements, *J. Geophys. Res.*, *99*, 10,341–10,356, 1994.

Koren, I., E. Ganor, and J. H. Joseph, On the relation between size and shape of desert dust aerosol, *J. Geophys. Res.*, *106*, 18,047–18,054, 2001.

Levin, Z., J. H. Joseph, and Y. Mekler, Properties of Sharav (Khamsin) dust-comparison of optical and direct sampling data, *J. Atmos. Sci.*, *37*, 882–891, 1980.

Li, X., H. B. Maring, D. Savoie, K. Voss, and J. M. Prospero, Dominance of mineral dust in aerosol light-scattering in the North Atlantic trade winds, *Nature*, *380*, 416–419, 1996.

Liao, H., and J. H. Seinfeld, Radiative forcing by mineral dust aerosols: sensitivity to key variables, *J. Geophys. Res.*, *103*, 31,637–31,645, 1998.

Livingston, J. M., et al., Airborne Sun photometer measurements of aerosol optical depth and columnar water vapor during the Puerto Rico Dust Experiment and comparison with land, aircraft, and satellite measurements, *J. Geophys. Res.*, *108*, doi:10.1029/2002JD002520, in press, 2003.

Maenhaut, W., J. Ptasinki, and J. Cafmeyer, Detailed mass size distributions of atmospheric aerosol species in the Negev Desert, Israel, during ARACHNE-96, *Nucl. Instrum. Methods Phys. Res.*, *150*, 422–427, 1999.

Maring, H. B., D. L. Savoie, M. A. Izaguirre, C. McCormick, R. Arimoto, J. M. Prospero, and C. Pilinis, Aerosol physical and optical properties and their relationship to aerosol composition in the free troposphere at Izania, Tenerife, Canary Islands, during July 1995, *J. Geophys. Res*, *105*, 14,677–14,700, 2000.

Maring, H., D. L. Savoie, M. A. Izaguirre, L. Custals, and J. S. Reid, Mineral dust aerosol size distribution change during atmospheric transport, *J. Geophys. Res.*, *108*, doi:10.1029/2002JD002536, in press, 2003a.

Maring, H., D. L. Savioe, M. A. Izaguirre, L. Custals, and J. S. Reid, Vertical distributions of dust and sea salt aerosols over Puerto Rico during PRIDE measured from a light aircraft, *J. Geophys. Res.*, *108*, doi:10.1029/2002JD002544, in press, 2003b.

Marple, V. A., K. L. Rubow, and B. A. Olsen, Inertial, gravitational, centrifugal, and thermal collection techniques, in *Aerosol Measurement: Principles, Techniques, and Applications*, edited by K. Willeke and P. A. Baron, pp. 345–380, Van Nostrand Reinhold, New York, 1993.

Marshall, I. A., J. P. Mitchell, and W. D. Griffiths, The behavior of regular-shaped non-spherical particles in a TSI aerodynamic particle sizer, *J. Aerosol Sci.*, *22*, 73–89, 1991.

Matsumoto, T., P. B. Russell, C. Mina, W. Van Ark, and V. Banta, Airborne tracking Sunphotometer, *J. Atmos. Oceanic Technol.*, *4*, 336–339, 1987.

Mishchenko, M. I., and L. D. Travis, Light scattering by polydispersions of randomly oriented spheroids with sizes comparable to wavelengths of observation, *Appl. Opt.*, *33*, 7206–7225, 1994.

Mishchenko, M. I., L. D. Travis, R. A. Kahn, and R. A. West, Modeling phase functions for dust-like tropospheric aerosols using a shape mixture of randomly oriented polydisperse spheroids, *J. Geophys. Res.*, *102*, 16,831–16,847, 1997.

Myhre, G., and F. Stordal, Global sensitivity experiments of the radiative forcing due to mineral aerosols, *J. Geophys. Res.*, *106*, 18,193–18,204, 2001.

Nakajima, T., M. Tanaka, M. Yamano, M. Shiobara, K. Arao, and Y. Nakanishi, Use of sky brightness measurements from ground or remote sensing of particulate polydispersions, *Appl. Opt.*, *35*, 2672–2689, 1996.

Patterson, E. M., Optical properties of the crustal aerosol: Relation to chemical and physical characteristics, *J. Geophys. Res.*, *86*, 3236–3246, 1981.

Patterson, E. M., and D. A. Gillette, Commonalties in measured size distribution for aerosol having a soil-derived component, *J. Geophys. Res.*, *82*, 2074–2082, 1977.

Pilinis, C., and X. Li, Particle shape and internal inhomogeneity effects on the optical properties of tropospheric aerosols of relevance to climate forcing, *J. Geophys. Res.*, *103*, 3789–3800, 1998.

Pinnick, R. G., and J. M. Rosen, Response of Knollenberg light-scattering counters to non-spherical doublet polystryrene latex aerosols, *J. Aerosol Sci.*, *10*, 533–538, 1979.

Porter, J., and A. D. Clarke, Aerosol size distribution models based on in situ measurements, *J. Geophys. Res.*, *102*, 6035–6045, 1997.

Quijano, A. L., I. N. Sokolik, and O. B. Toon, Influence of the aerosol vertical distribution on the retrievals of aerosol optical depth from satellite radiance measurements, *Geophys. Res. Lett.*, *27*, 3457–3460, 2000a.

Quijano, A. L., I. N. Sokolik, and O. B. Toon, Radiative heating rates and direct radiative forcing by mineral dust in cloudy atmospheric conditions, *J. Geophys. Res.*, *105*, 12,207–12,219, 2000b.

Rader, D. J., and T. J. O'Hern, Optical direct reading techniques: In situ sampling, in *Aerosol Measurement: Principles, Techniques, and Applications*, edited by K. Willeke and P. A. Baron, pp. 345–380, Van Nostrand Reinhold, New York, 1993.

Reid, E. A., J. S. Reid, M. M. Meyer, M. Dunlop, S. S. Cliff, A. Broumas, K. D. Perry, and H. Maring, Characterization of African dust transported to Puerto Rico by individual particle and size segregated bulk analysis, *J. Geophys. Res.*, *108*, doi:10.1029/2002JD002935, in press, 2003.

Reid, J. S., T. A. Cahill, and M. R. Dunlap, Geometric/aerodynamic size ratios of ash aggregates from burning Kuwaiti oil fields, *Atmos. Environ.*, *28*, 2227–2234, 1994a.

Reid, J. S., R. G. Flocchini, T. A. Cahill, R. S. Ruth, and D. P. Salgado, Local meteorological, transport, and source aerosol characteristics of late Autumn Owens Lake (dry) dust storms, *Atmos. Environ.*, *28*, 1699–1706, 1994b.

Reid, J. S., W. L. Westphal, J. Livingston, D. S. Savoie, H. B. Maring, P. Pilewskie, and D. Eleuterio, The vertical distribution of dust transported into the Caribbean during the Puerto Rico Dust Experiment, *Geophys. Res. Lett.*, *29*(7), 1151, doi:10.1029/2001GL014092, 2002.

Reid, J. S., et al., Analysis of measurements of Saharan dust by airborne and ground-based remote sensing methods during the Puerto Rico Dust Experiment (PRIDE), *J. Geophys. Res.*, *108*, doi:10.1029/2002JD002493, in press, 2003.

Schulz, M., Y. J. Balanski, W. Guelle, and F. Dulac, Role of aerosol size distribution and source location in a three-dimensional simulation of a Saharan dust episode tested against satellite-derived optical thickness, *J. Geophys. Res.*, *103*, 10,579–10,592, 1998.

Shettle, E. P., and R. W. Fenn, Models for the aerosols of the lower atmosphere and the effects of humidity variations on their optical properties, *AFGL-TR-79-0214*, 94 pp., Air Force Res. Lab., Wright-Patt Air Force Base, Ohio, 1979.

Smirnov, A., B. N. Holben, I. Slutsker, E. J. Welton, and P. Formenti, Optical properties of Saharan dust during ACE-2, *J. Geophys. Res.*, *103*, 28,079–28,092, 1998.

Smirnov, A., B. N. Holben, T. F. Eck, O. Dubovik, and I. Slutsker, Cloud screening and quality control algorithms for the AERONET database, *Remote Sens. Environ.*, *73*, 337–349, 2000.

Smirnov, A., B. N. Holben, O. Dubovik, N. T. O'Neal, T. F. Eck, D. L. Westphal, A. K. Goroch, C. Pietras, and I. Slutsker, Atmospheric aerosol optical properties in the Persian Gulf, *J. Atmos. Sci.*, *59*, 620–634, 2002.

Sokolik, I. N., and O. B. Toon, Incorporation of mineralogical composition into models of the radiative properties of mineral aerosols from UV to IR wavelengths, *J. Geophys. Res.*, *104*, 9423–9444, 1999.

Sviridenkov, D., A. Gillette, A. A. Isakov, I. N. Sokolik, V. V. Smirnov, B. D. Belan, M. V. Pachenko, A. V. Andronova, S. M. Kolomits, V. M. Zhukov, and D. A. Zhukovsky, Size distributions of dust aerosol measured during the Soviet-American Experiment in Tadzhikistand, 1989, *Atmos. Environ., Part A*, *27*, 2481–2486, 1993.

Talbot, R. W., R. C. Harriss, E. V. Browell, G. L. Gregory, D. I. Sebacher, and S. M. Beck, Distribution and geochemistry in the tropical North Atlantic Troposphere: Relationship to dust, *J. Geophys. Res.*, *91*, 5173–5182, 1986.

Tanre, D., Y. J. Kaufman, B. N. Holben, B. Chatenet, A. Karnieli, F. Lavenu, L. Blarel, O. Dubovik, L. A. Remer, and A. Smirnov, Climatology of dust aerosol size distribution and optical properties derived from remotely sensed data in the solar spectrum, *J. Geophys. Res.*, *106*, 18,205–18,219, 2001.

Taylor, S. R., and S. M. McLennan, The geochemical evolution of the continental crust, *Rev. Geophys.*, *33*, 241–265, 1995.

Tegen, I., and A. A. Lacis, Modeling of particle size distribution and its influence on the radiative properties of mineral dust aerosol, *J. Geophys. Res.*, *101*, 19,237–19,244, 1996.

Westphal, D. L., O. B. Toon, and T. N. Carlson, A two-dimensional numerical investigation of the dynamics and microphysics of Saharan dust storms, *J. Geophys. Res.*, *92*, 3027–3049, 1987.

S. S. Cliff, DELTA Group, Applied Science, University of California, Davis, CA 95616, USA.

O. Dubovik and A. Smirnov, GEST Center, University of Maryland Baltimore County, Baltimore, MD 21250, USA.

H. H. Jonsson, Naval Postgraduate School, Monterey, CA 93943, USA.

J. M. Livingston, SRI International, Palo Alto, CA 94025, USA.

H. B. Maring and D. L. Savoie, Rosenstiel School of Marine and Atmospheric Science, University of Miami, Miami, FL 33149, USA.

M. M. Meier, Material Science and Chemical Engineering, University of California, Davis, CA 95616, USA.

E. A. Reid and J. S. Reid, Naval Research Laboratory, 7 Grace Hopper Street, Monterey, CA 93943-5502, USA. (reidj@nrlmry.navy.mil)

S.-C. Tsay, NASA Goddard Space Flight Center, Greenbelt, MD 20771, USA.